

Supporting Information

Atomically Dispersed Ru on Manganese Oxide Catalyst Boosts Oxidative Cyanation

Hai Wang,^{a,#} Dongyang Xu,^{b,#} Erjia Guan,^{c,#} Liang Wang,^{a,*} Jian Zhang,^e Chengtao Wang,^d Sai Wang,^d Hua Xu,^d Xiangju Meng,^d Bo Yang,^{b,*} Bruce C. Gates,^c and Feng-Shou Xiao^{a,d,e,*}

^aKey Lab of Biomass Chemical Engineering of Ministry of Education College of Chemical and Biological Engineering, Zhejiang University, Hangzhou 310027, China.

^bSchool of Physical Science and Technology, ShanghaiTech University, Shanghai 201210, China

^cDepartment of Chemical Engineering, University of California, Davis CA 95616, United States

^dKey Lab of Applied Chemistry of Zhejiang Province, Department of Chemistry, Zhejiang University, Hangzhou 310028, China.

^eBeijing Advanced Innovation Center for Soft Matter, Science and Engineering, Beijing University of Chemical Technology, Beijing 100029, China

*Corresponding author: liangwang@zju.edu.cn; yangbo1@shanghaitech.edu.cn; fsxiao@zju.edu.cn

H. Wang, D. Xu, and E. Guan contributed equally.

Experimental details

Chemicals

All chemicals were of analytical grade and used without further purification. KMnO₄ and MnSO₄·H₂O were purchased from Sino-Pharm Chemical Reagent Co., Ltd (AR). CeO₂ (Cat. No. C103981-500G), MnO (Cat. No. M105456-500G), commercial Activated-MnO₂ (Cat. No. M118110-10G, denoted as A-MnO₂), Co₃O₄ (Cat. No. C111615-25G), Mn₃O₄ (Cat. No. M111159-250G), Mn₂O₃ (Cat. No. M832185-100G), SiO₂ (Cat. No. E1712057-250G), and Al₂O₃ (Cat. No. G1724058-100G) were commercial products from Aladdin Chemical Company. Benzyl alcohol, *n*-heptanol, hexane-1,6-diol, hexan-1-ol, 1-nonal, 1-decanol, 2-methoxybenzyl alcohol, 3-methoxybenzyl alcohol, 4-methoxybenzyl alcohol, 4-fluorobenzyl alcohol, 4-chlorobenzyl alcohol, 4-bromobenzyl alcohol, [4-(trifluoromethyl) phenyl]methanol, 4-methylbenzyl alcohol, furfuryl alcohol, 3-pyridinemethanol, 3-thiophenemethanol, (2-naphthyl)methanol, 4-nitrobenzyl alcohol, cinnamyl alcohol, Methyl 4-(hydroxymethyl) benzoate and the corresponding nitrile products were obtained from Aladdin Chemical Company, TCI, and J&K China Chemical Ltd.

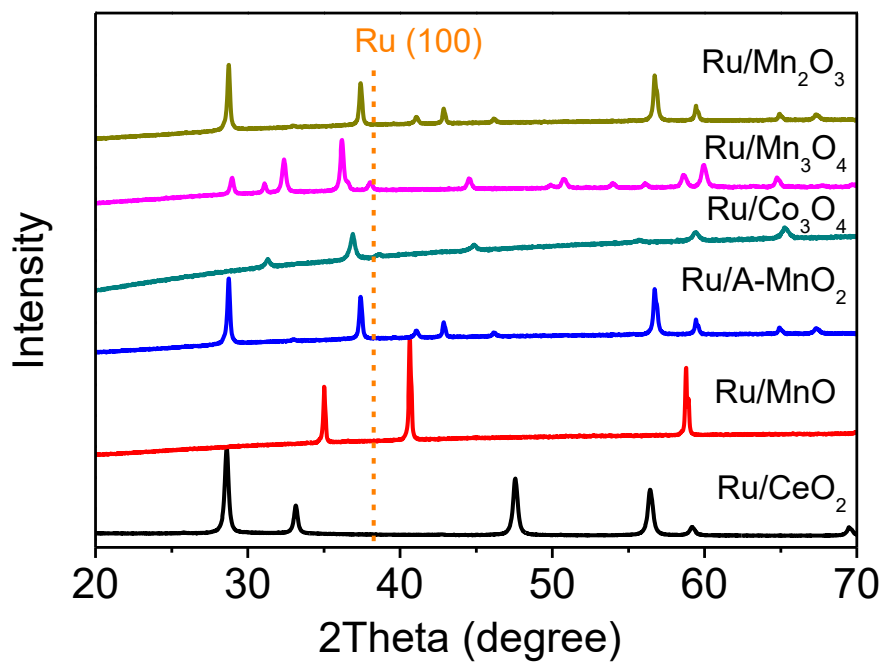


Figure S1. XRD patterns of various catalysts with Ru loading of 0.1 wt%.

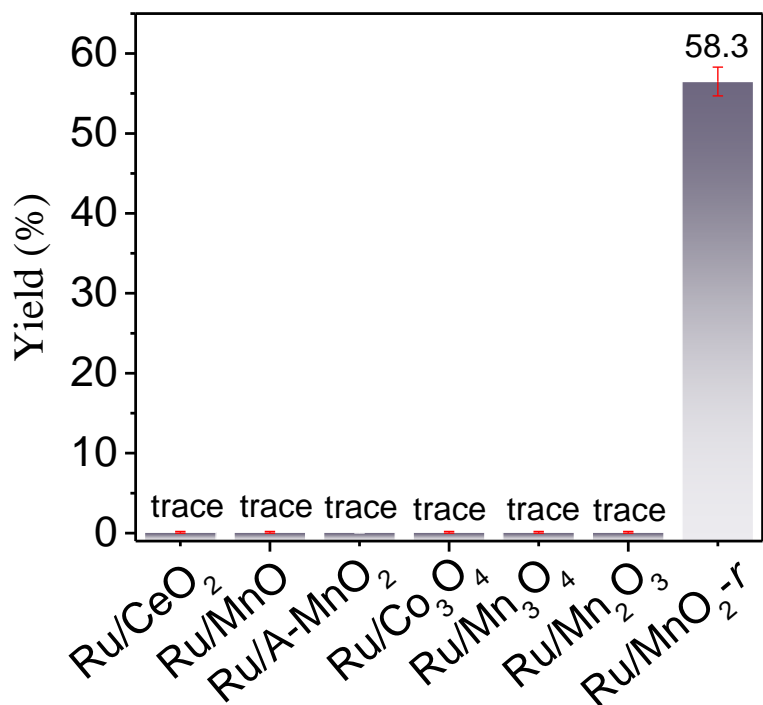


Figure S2. Oxidative cyanation of *n*-heptanol in the presence of various catalysts with Ru loadings of 0.1 wt%. Reaction conditions: 0.2 mmol of substrate, 4 mL of *t*-amyl alcohol solvent, 100 µL of aqueous NH₃ (28-30 wt%), 100 mg of catalyst, 2.0 MPa of oxygen, 100 °C, 2 h. Yield: yield to heptanenitrile. More data are presented in Table S2.

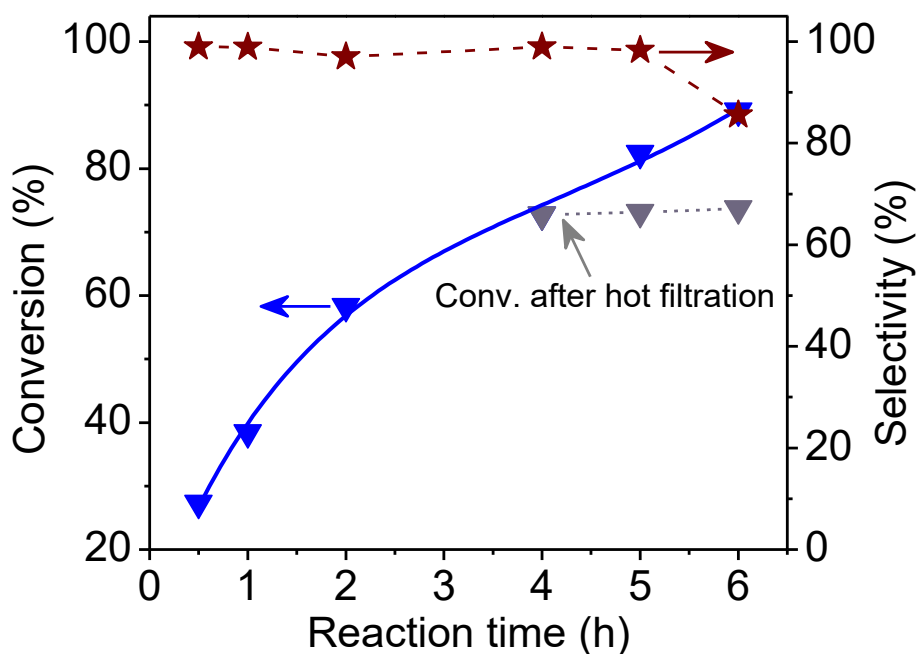


Figure S3. Conversion of *n*-heptanol in a batch reactor catalyzed by 0.1Ru/MnO₂-*r* in the oxidative cyanation of *n*-heptanol. Reaction conditions: 0.2 mmol of *n*-heptanol, 100 mg of 0.1Ru/MnO₂-*r*, 4 mL of *t*-amyl alcohol solvent, 100 μL of aqueous NH₃ (28–30 wt%), 2.0 MPa of oxygen, 100 °C. The solid line in blue: the general reaction for 6 h; the dotted line in gray: the solid catalyst was removed after 4 h, the blue lines and gray lines correspond to data taken in two separate experiments.

Note: After removing the solid catalyst from the reaction liquor at 4 h, the conversion of *n*-heptanol remained unchanged with further reaction, indicating that the negligible leaching of 0.1Ru/MnO₂-*r* under the reaction conditions.

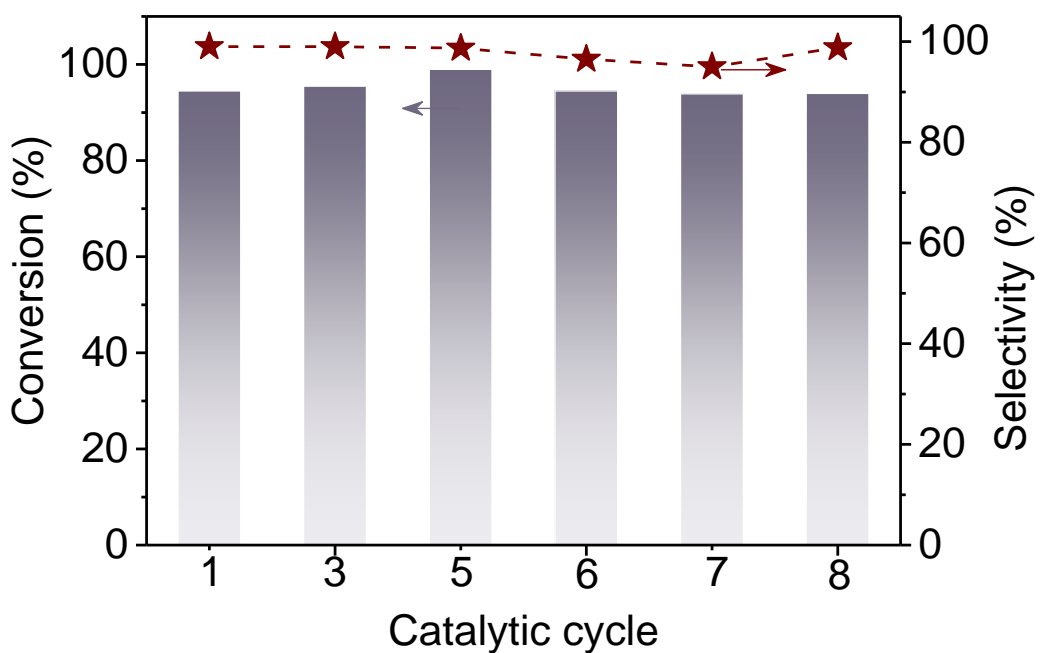


Figure S4. Recycling tests of 0.1Ru/MnO₂-*r* in the oxidative cyanation of benzyl alcohol to benzonitrile. Reaction conditions: 2.4 mmol of benzyl alcohol, 16 mL of *t*-amyl alcohol solvent, 600 μL of aqueous NH₃ (28-30 wt%), 300 mg of catalyst, 1.5 MPa of oxygen, 75 °C.

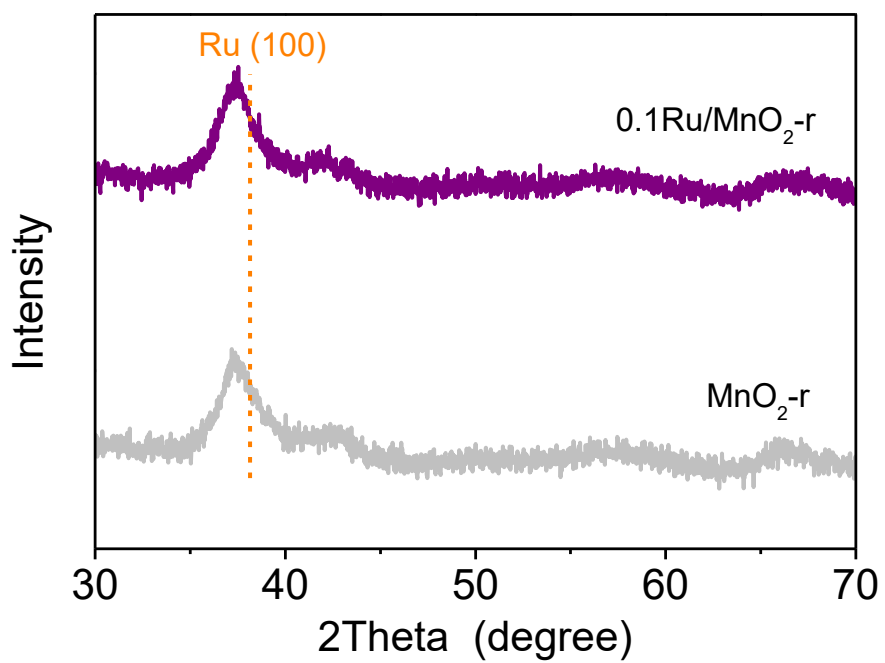


Figure S5. XRD patterns of $\text{MnO}_2\text{-}r$ and $0.1\text{Ru}/\text{MnO}_2\text{-}r$.

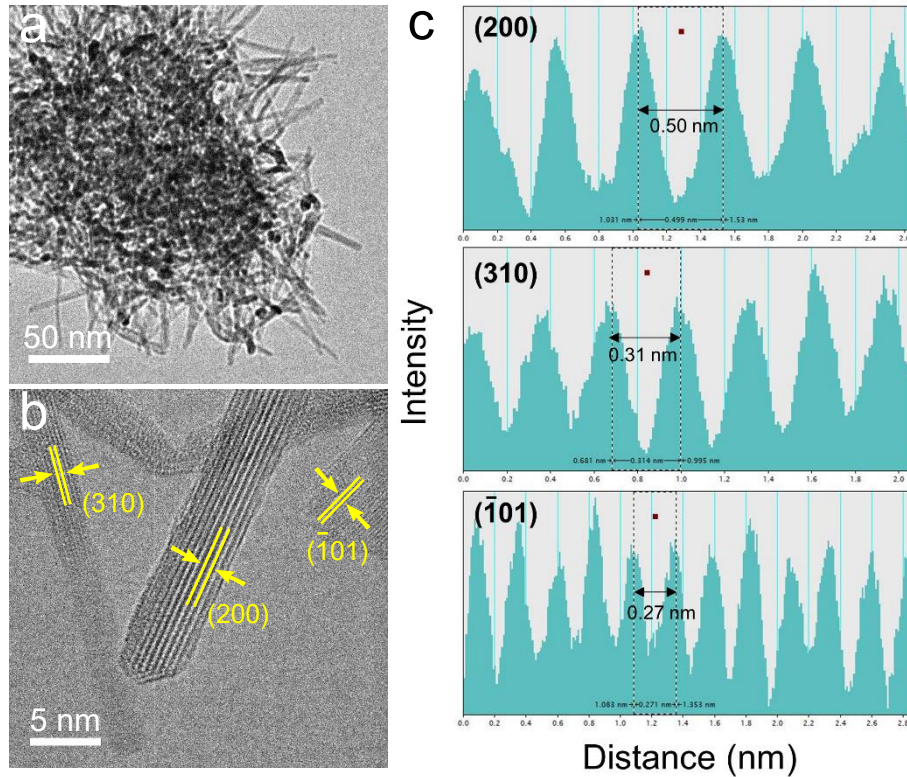


Figure S6. (a) TEM and (b) high-resolution TEM images of MnO₂-r. (c) Measurement of the lattice.

Note: TEM characterization of the MnO₂-r shows the nanorod morphology with average size at about 4.9 nm. The high-resolution transmission electronic microscopic (HRTEM) image shows the lattice spacing at 0.50, 0.31, and 0.27 nm that correspond to the (200), (310), and (-101) planes of α -MnO₂ structure, respectively.¹⁻⁴

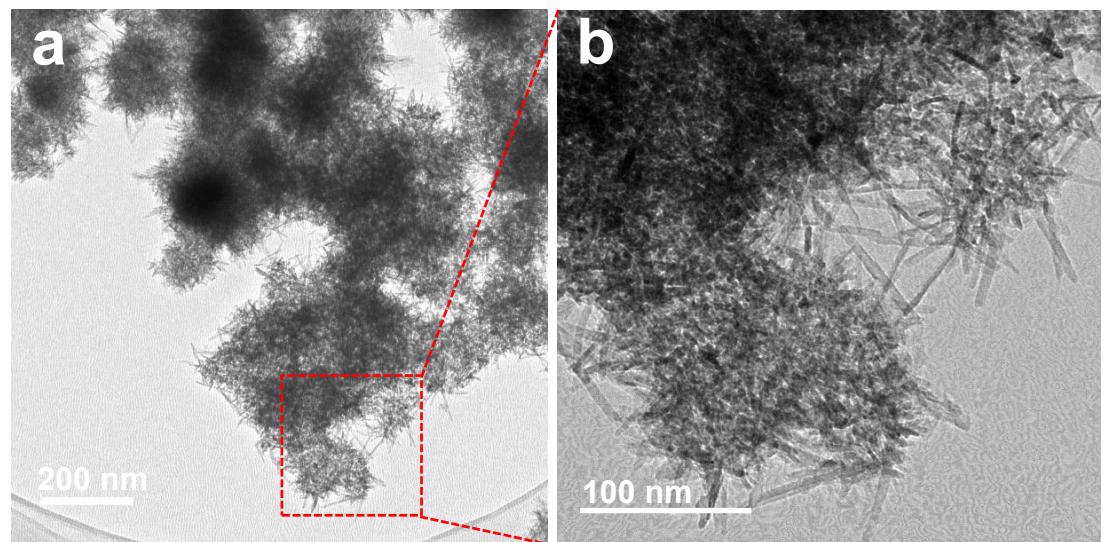


Figure S7. (a) TEM images of $0.1\text{Ru}/\text{MnO}_2\text{-}r$. (b) Enlarged view of the region shown in the red square in (a).

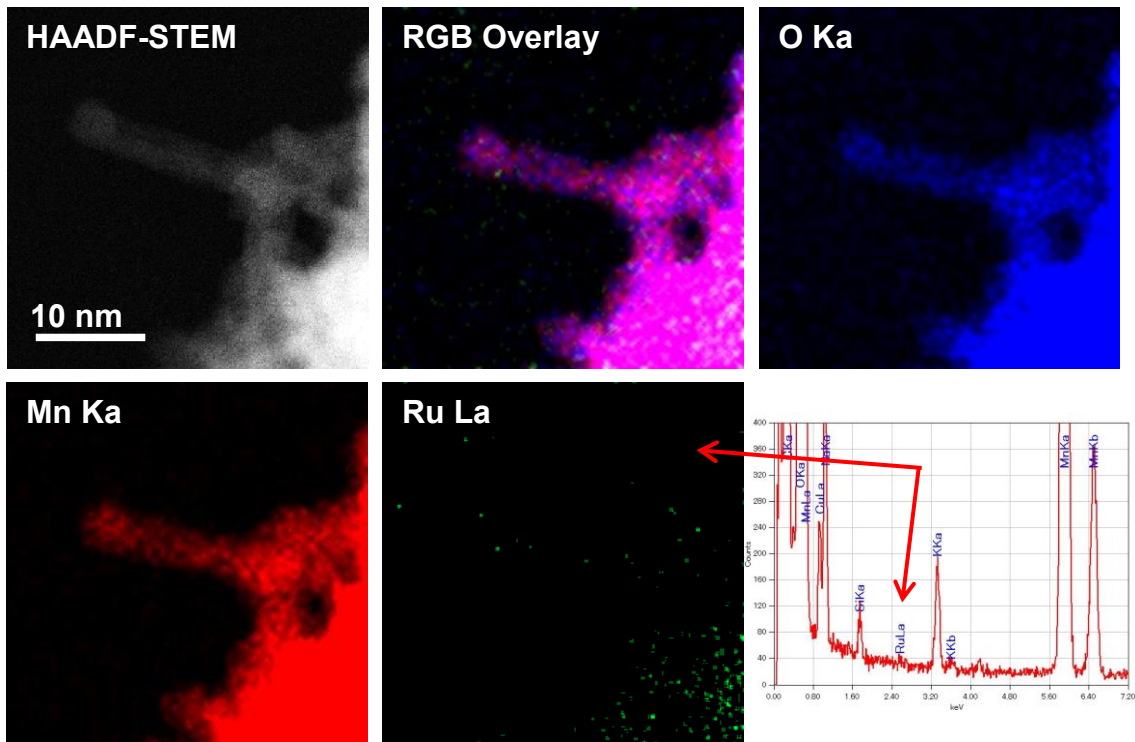


Figure S8. HAADF-STEM image and the corresponding elemental maps of 0.1Ru/MnO₂-*r* catalyst.

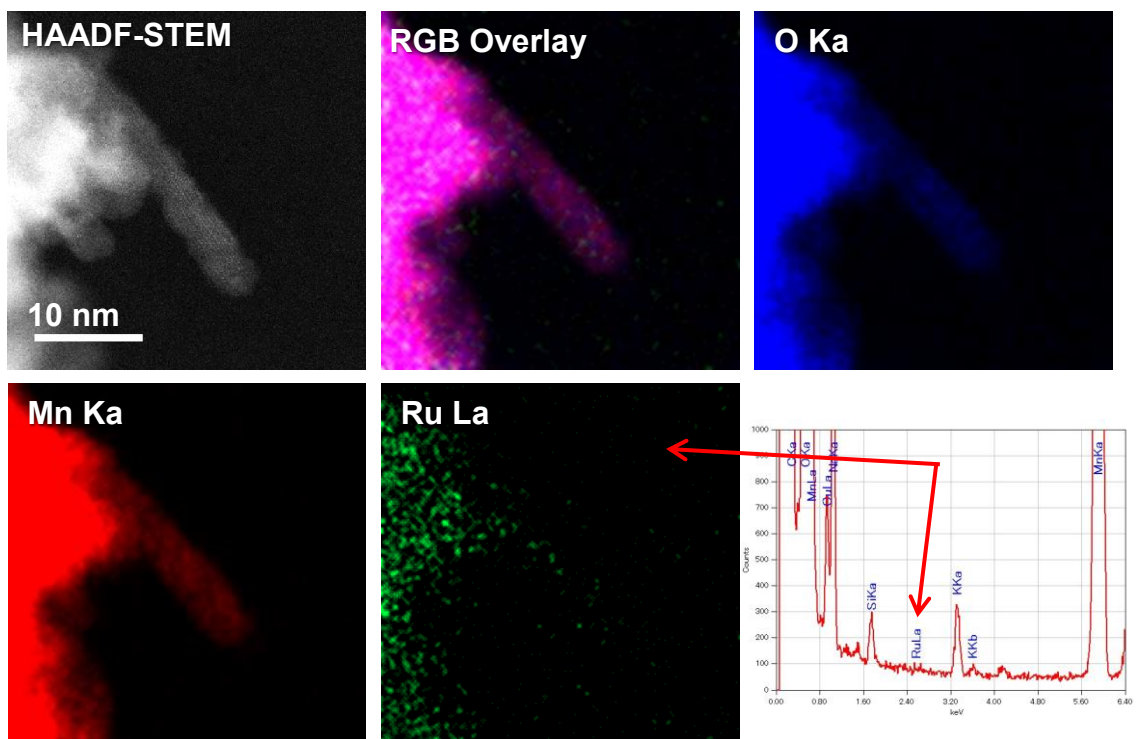


Figure S9. HAADF-STEM image and the corresponding elemental maps for the 0.1Ru/MnO₂-*r* catalyst. The randomly selected region is different from that in Figure S8.

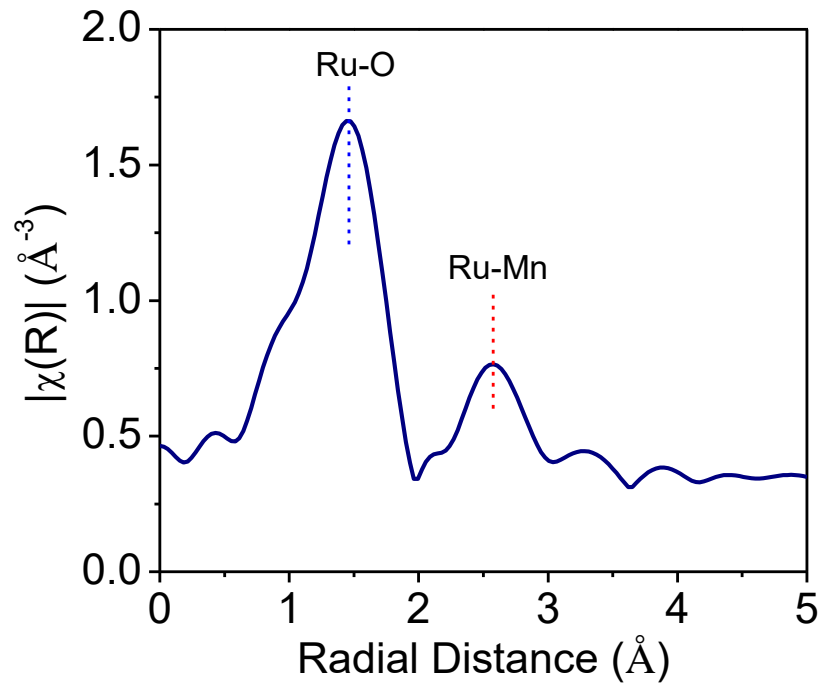


Figure S10. Ru *K*-edge EXAFS spectra in *R*-space of 3.0Ru/MnO₂-*r*. For this sample with the high Ru loading of 3.0 wt%, the Ru is still dispersed in single sites.

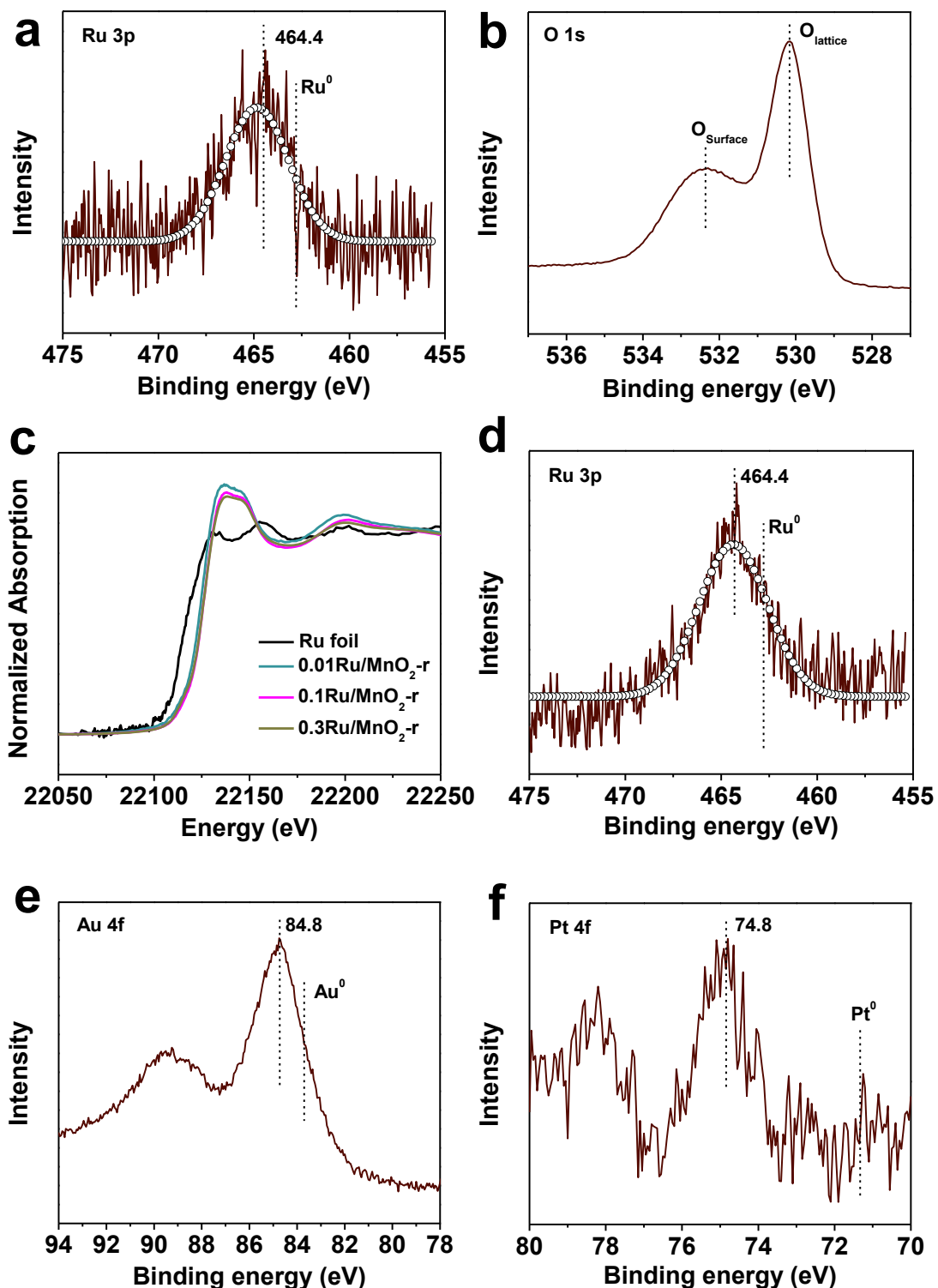


Figure S11. (a) Ru 3p and (b) O 1s XP spectra of Ru/MnO₂-r catalyst; (c) Ru K-edge XANES spectra of various Ru-catalysts; (d) Ru 3p XP spectra of the spent Ru/MnO₂-r catalyst; (e) Au 4f XP spectra of Au/MnO₂-r catalyst; (f) Pt 4f XP spectra of Pt/MnO₂-r catalyst.

Note: After the reaction, the spent Ru/MnO₂-*r* catalyst still exhibited Ru 3p binding energy at 464.4 eV (Figure S11d), which is almost unchanged compared with the as-synthesized catalyst.

Similar to the Ru in the Ru catalyst, the Au and Pt species also show a positively charged state when localized on MnO₂-*r* (Figures S11e and S11f), which also originated from the interaction with MnO₂-*r* support.⁵⁻¹⁴

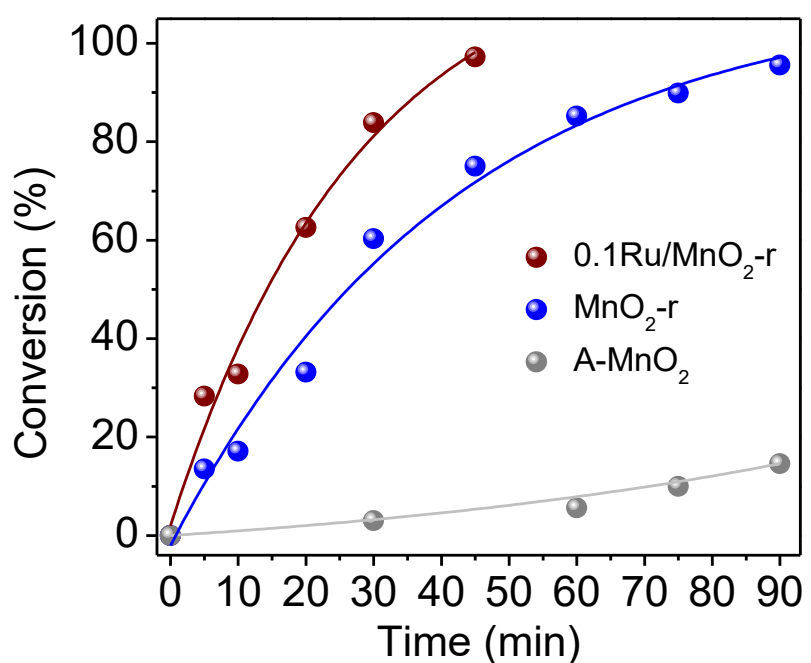


Figure S12. Benzyl alcohol conversions in a batch reactor catalyzed by A-MnO₂, MnO₂-r, and 0.1Ru/MnO₂-r. Reaction conditions: 0.4 mmol of benzyl alcohol, 50 mg of catalyst, 4 mL of *t*-amyl alcohol solvent, 100 μ L of aqueous NH₃ (28-30 wt%), 1.5 MPa of O₂, 75 °C.

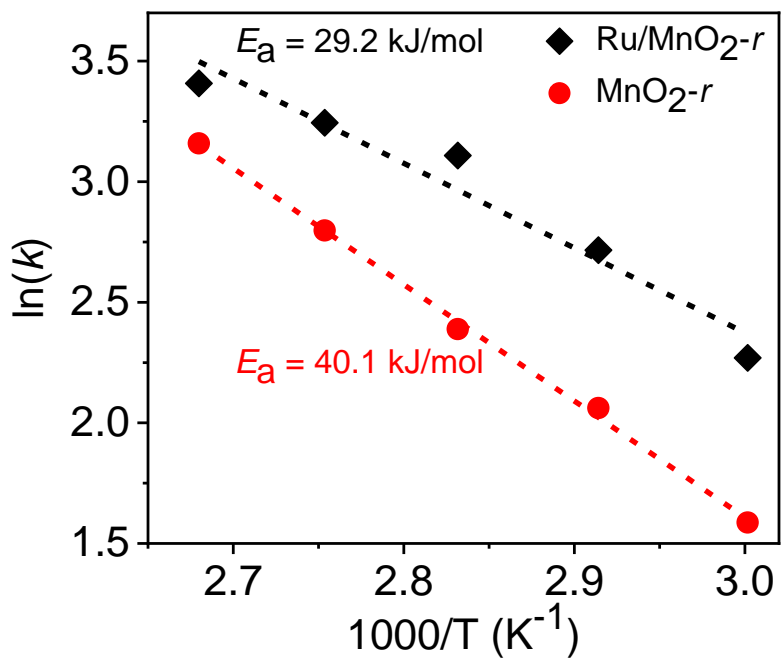


Figure S13. Arrhenius plots for the benzyl alcohol dehydrogenation catalyzed by 0.1Ru/MnO₂-*r* and MnO₂-*r*. Reaction conditions: 0.4 mmol of benzyl alcohol, 4 mL of *t*-amyl alcohol solvent, 100 µL of aqueous NH₃ (28–30 wt%), 1.5 MPa of oxygen. The conversions were lower than 20% for calculating the average reaction rates, which, in the limit as conversion approaches zero, approach true reaction rates.

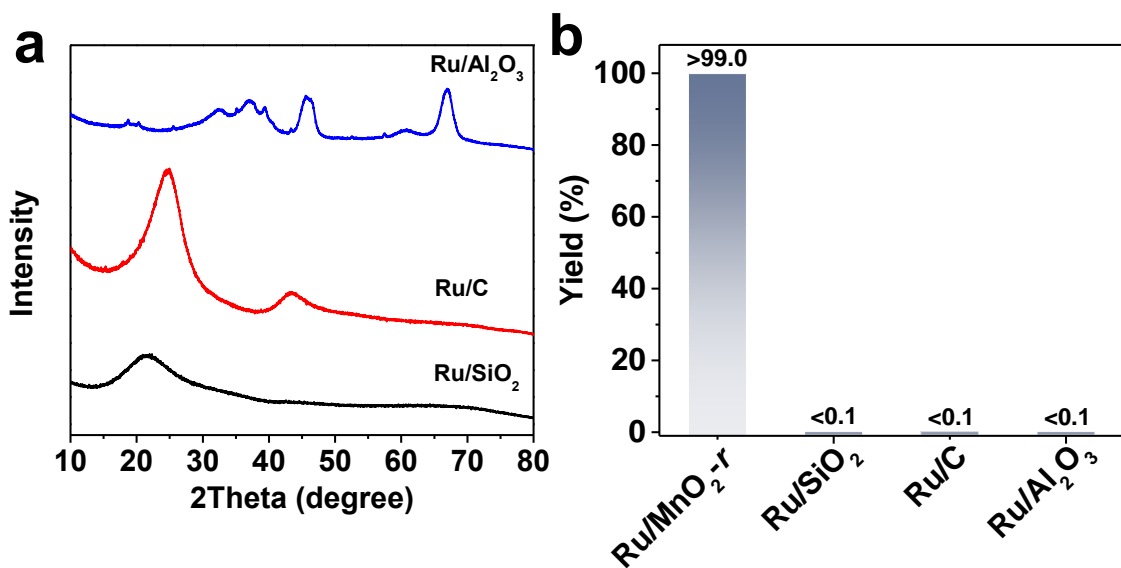


Figure S14. (a) XRD patterns of various catalysts with Ru loading amount at 0.1 wt%.

(b) Catalytic data in oxidative cyanation of benzyl alcohol on various catalysts. Yield: yield to benzonitrile. Reaction conditions: 0.4 mmol of benzyl alcohol, 4 mL of *t*-amyl alcohol, 100 μL of aqueous NH₃ (28-30 wt%), 10 mg of catalysts, 0.5 MPa of O₂, 100 °C, 5 h.

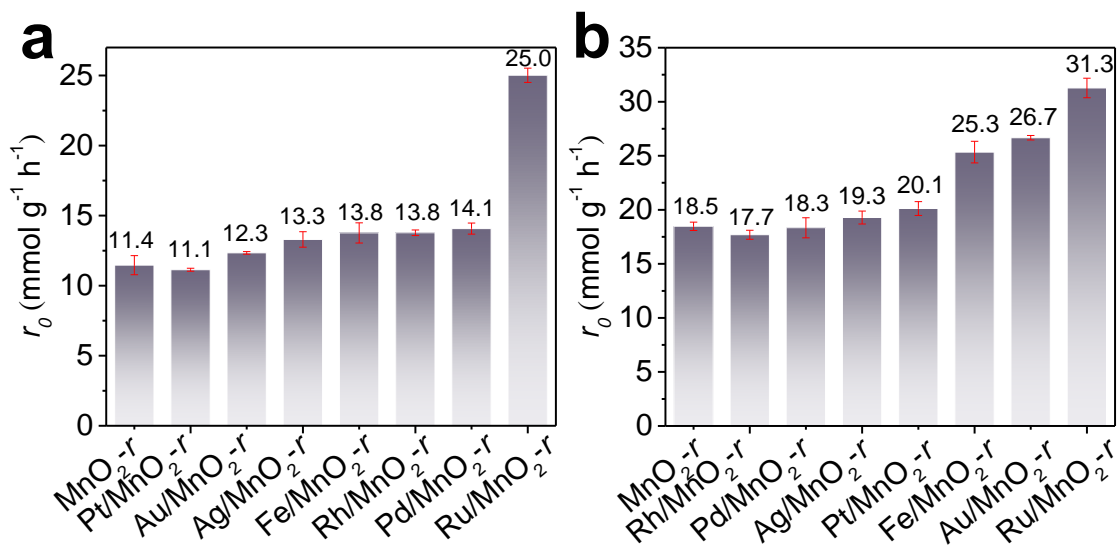


Figure S15. Average reaction rates (r_0) characterizing various catalysts in the oxidative cyanation of (a) benzyl alcohol and (b) benzaldehyde. Reaction conditions: 0.4 mmol of substrate, 50 mg of catalyst, 4 mL of *t*-amyl alcohol solvent, 100 μ L of aqueous NH₃ (28-30 wt%), 1.5 MPa of O₂, 75 °C. Metal content of catalysts: 0.3 wt% for all the catalysts except MnO₂-*r*.

Note: The average rates of benzaldehyde conversion are always higher than that of benzyl alcohol under the same reaction conditions with various catalysts, indicating that the alcohol dehydrogenation may be rate-determining in the alcohol oxidative cyanation process. Furthermore, the Ru/MnO₂-*r* exhibits higher activity for the rate-determining reaction than the other catalysts.

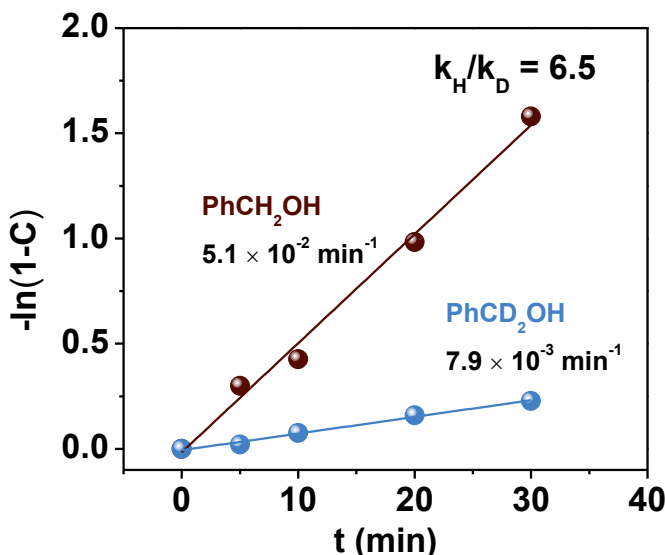


Figure S16. Time-on-stream course of conversion. Reaction conditions: 0.4 mmol of benzyl alcohol/ α -deuterated benzyl alcohol, 4 mL of *t*-amyl alcohol, 100 μ L of aqueous NH₃ (28–30 wt%), 50 mg of 0.1Ru/MnO₂-*r*, 1.5 MPa of O₂, 75 °C. C: conversion of benzyl alcohol.

Note: The H/D KIE and kinetics of the reactions, including the rate constant and reaction order were studied. Assuming that the oxidation of benzyl alcohol follows the first-reaction kinetic law, that is $\ln[1/(1-C)] = k(t - t_0)$, where C is the conversion of benzyl alcohol (mol %), k is the rate constant (min^{-1}), and t represents reaction time (min), and a linear relationship between $-\ln(1 - C)$ and reaction time (min) was obtained, indicating that the reaction is first order with respect to benzyl alcohol,¹⁵ and the rate constant k_H for PhCH₂OH at 75 °C is $5.1 \times 10^{-2} \text{ min}^{-1}$. Additionally, H/D kinetic isotope effects (KIE) for the oxidation of benzyl alcohol (PhCH₂OH) and α -deuterated benzyl alcohol (PhCD₂OH) was evaluated and rate constant k_D for PhCD₂OH at 75 °C is $k_D = 7.9 \times 10^{-3} \text{ min}^{-1}$, thus giving a large value of k_H/k_D at 6.5.

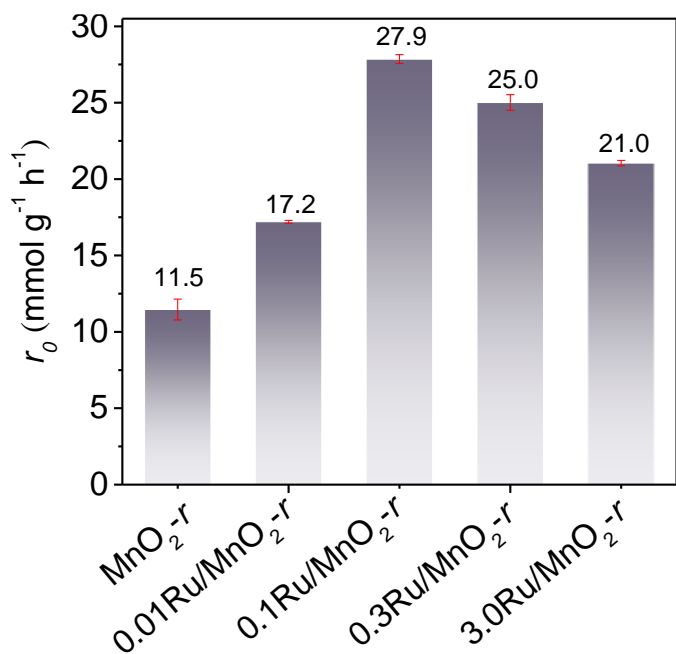


Figure S17. Average reaction rates (r_0) observed with various catalysts in the oxidative cyanation of benzyl alcohol. Reaction conditions: 0.4 mmol of benzyl alcohol, 50 mg of catalyst, 4 mL of *t*-amyl alcohol solvent, 100 μL of aqueous NH_3 (28–30 wt%), 1.5 MPa of O_2 , 75 °C.

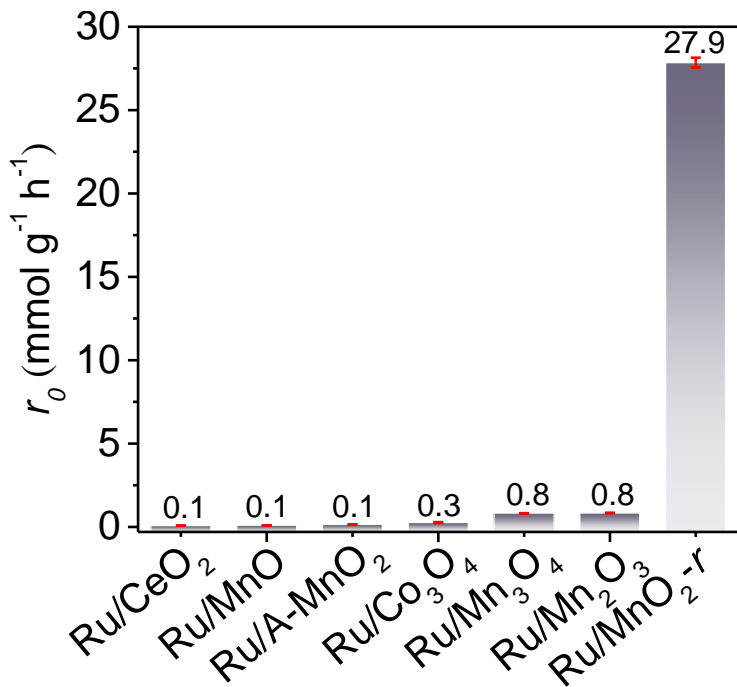


Figure S18. Average reaction rates (r_0) observed with various catalysts in the oxidative cyanation of benzyl alcohol. Reaction conditions: 0.4 mmol of benzyl alcohol, 50 mg of catalyst, 4 mL of *t*-amyl alcohol solvent, 100 μ L of aqueous NH₃ (28-30 wt%), 1.5 MPa of O₂, 75 °C. Ru loading content was 0.1 wt% for all the catalysts.

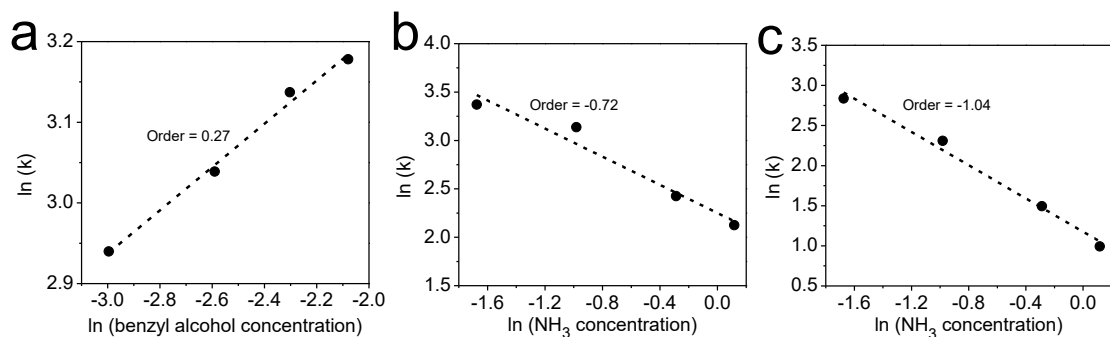


Figure S19. Plots determining reaction orders for the conversion of benzyl alcohol to benzonitrile of (a) benzyl alcohol and (b) NH_3 on $0.1\text{Ru}/\text{MnO}_2-r$ and (c) NH_3 over MnO_2-r . Reaction conditions: 0.2–0.5 mmol of substrate, 4 mL of *t*-amyl alcohol solvent, 50–300 μL of aqueous NH_3 (28–30 wt%), 1.5 MPa of oxygen, 50 mg of catalyst.

Note: As shown in Figure S19a, the positive order of reaction in benzyl alcohol (0.27) indicates that its activation may be involved in the rate-determining step, which is also confirmed by our H/D kinetic isotope effect (KIE) study (Figure S16) and DFT simulations (Figure 6).^{16,17} The reaction order in NH_3 is -0.72 for reaction on $0.1\text{Ru}/\text{MnO}_2-r$ (Figure S19b), confirming that more ammonia species might inhibit the catalysis.^{17,18} In contrast, the reaction order in NH_3 is -1.04 on the Ru-free MnO_2-r catalyst (Figure S19c). The difference between these values might also be suggested to confirm the enhanced ammonia resistance after the addition of Ru species to the MnO_2-r .

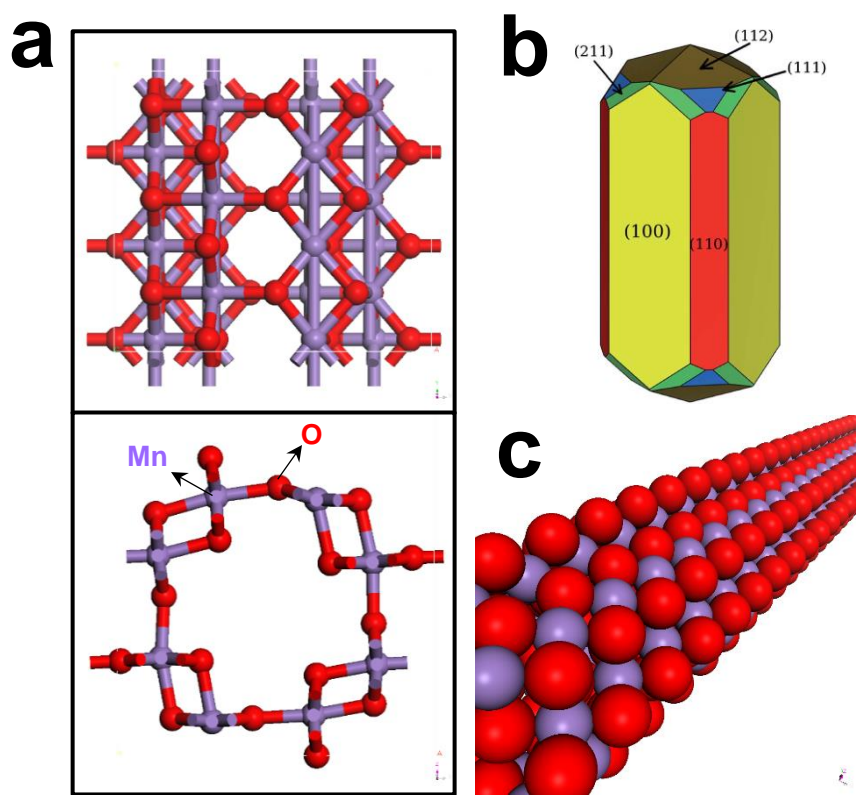


Figure S20. (a) The optimized structure and (b and c) models of the nanorod MnO_2 support.¹⁹

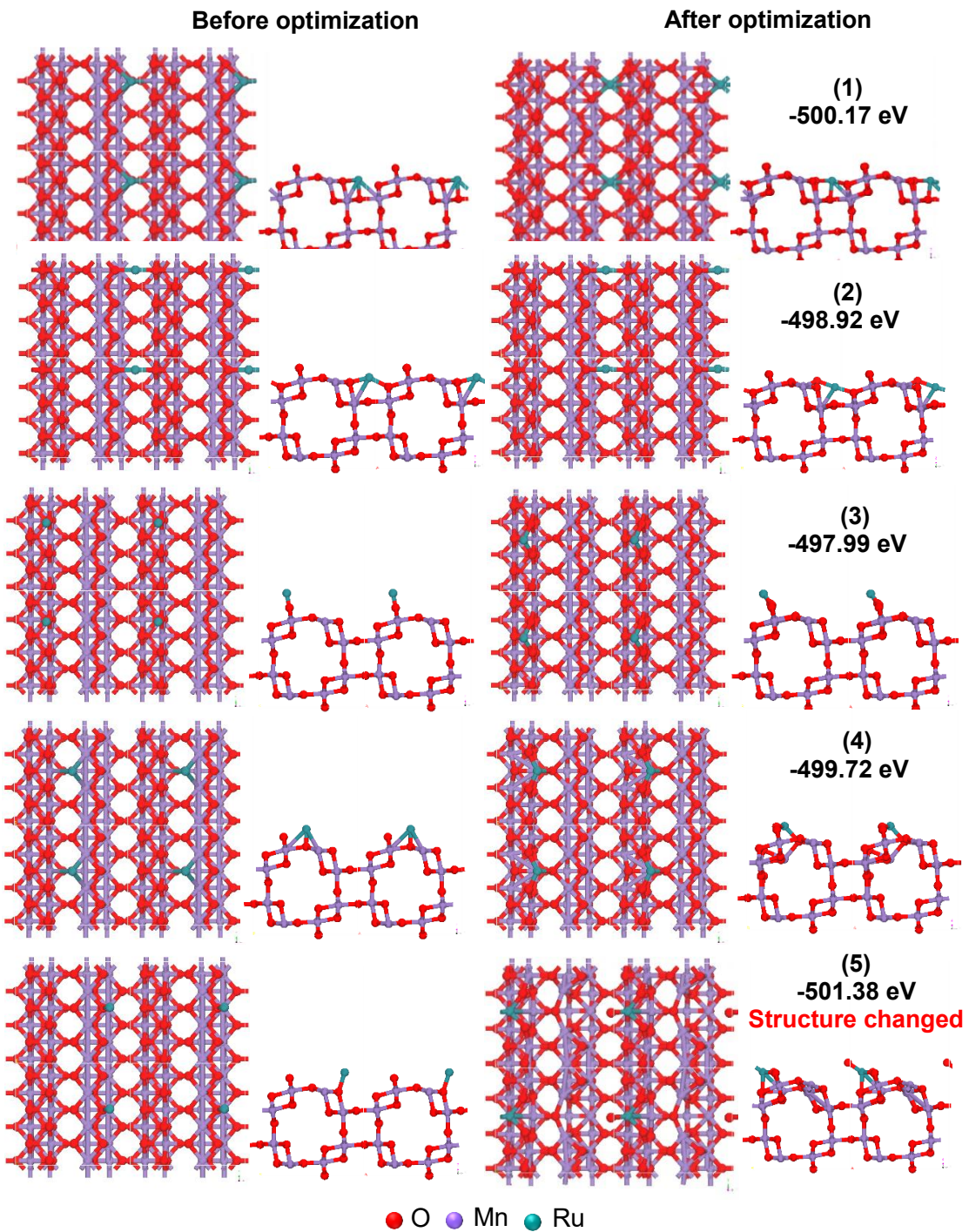


Figure S21. Several configurations of the $\text{MnO}_2\text{-}r$ supported single site Ru ($\text{Ru}/\text{MnO}_2\text{-}r$).

Note: The computational modeling used the lattice structure of $\alpha\text{-MnO}_2$ according to the XRD experiment results presented in Figure S5. It was also reported that the (100) surface dominates and represents 54% of the $\alpha\text{-MnO}_2$ surface area with low energies of

0.64 J m^{-2} .¹² In addition, the single atom model used in the simulation is supported by the EXAFS and HAADF-STEM results (Figure 4 in the main text). Several configurations of the supported single atoms were considered and the energy and structural stability for these configurations were evaluated after the geometrical optimization. As shown in Figure S21, the first configuration with an energy of -500.17 eV is the most stable one in these models. On the basis of the correlation to experimental results and theoretical optimization, the first model of single-site Ru on MnO_2-r was used for the theoretical investigation in this work.

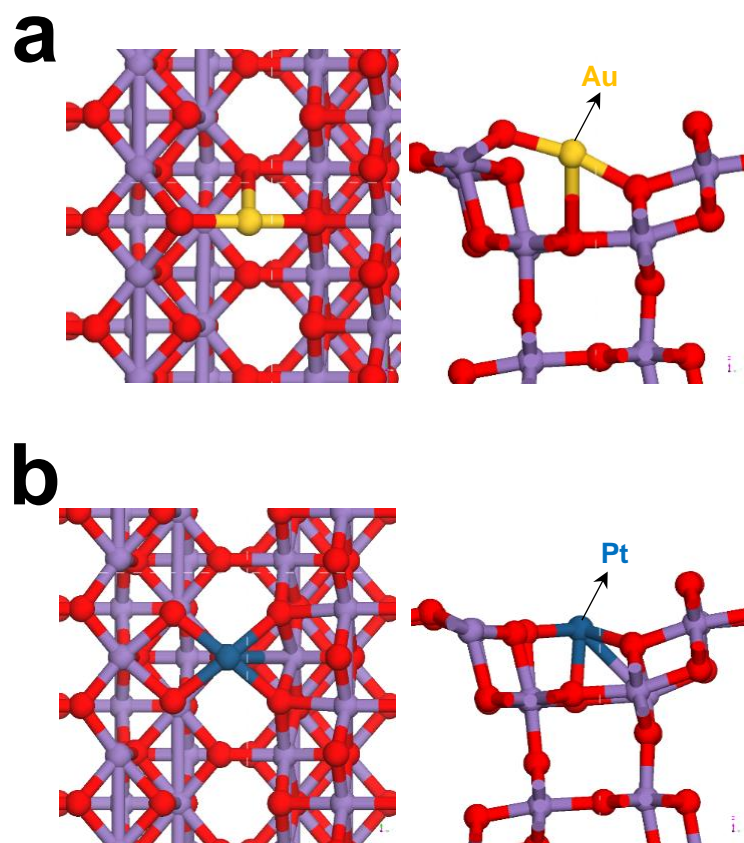


Figure S22. The optimized structures of single-site (a) Au and (b) Pt anchored on $\text{MnO}_2\text{-}r$.

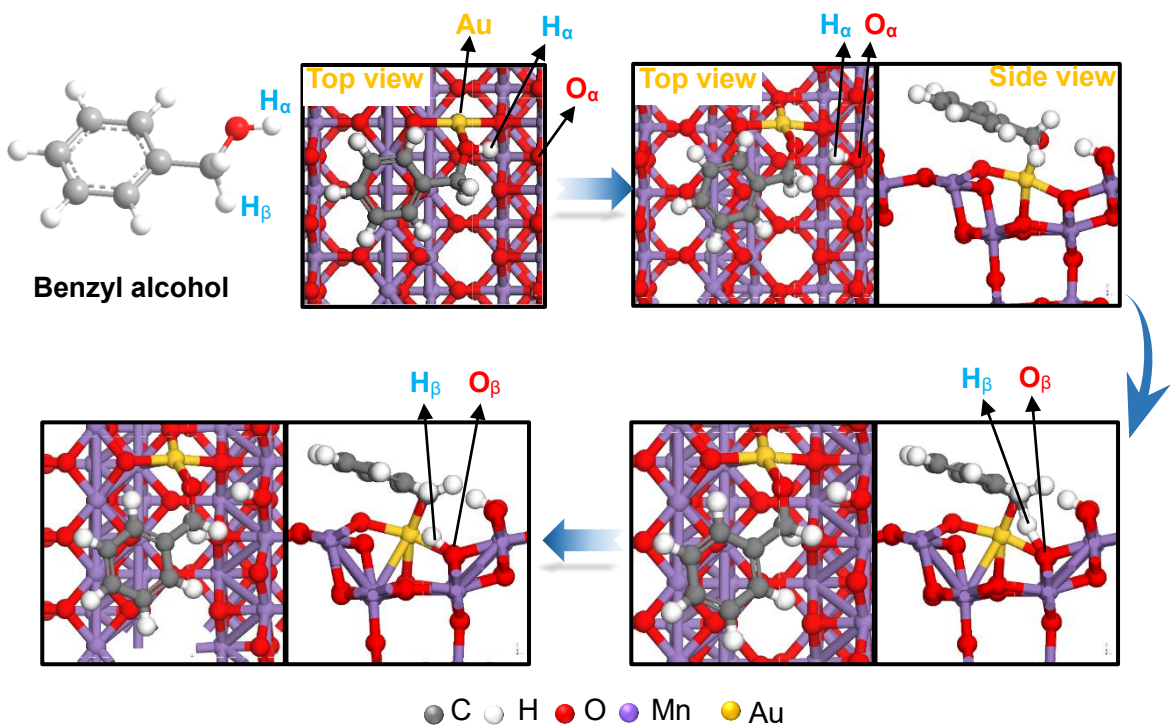


Figure S23. The proposed steps for PhCH_2OH dehydrogenation on Au/MnO_2-r model.

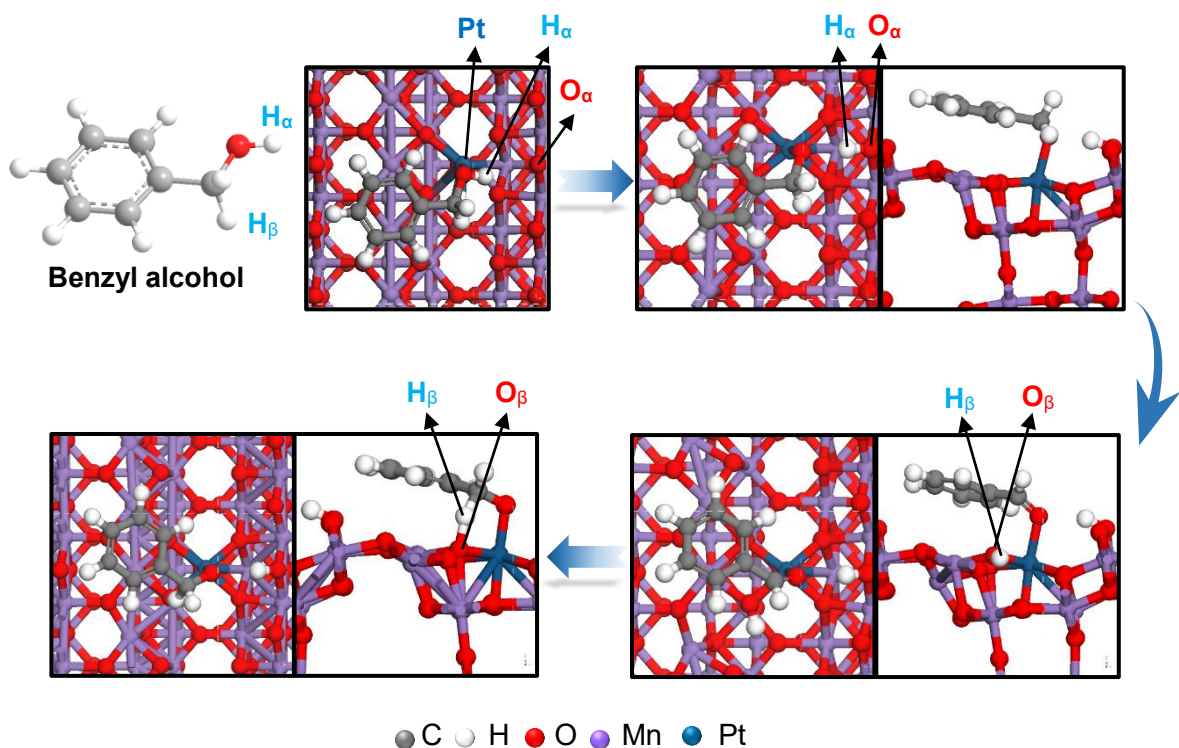


Figure S24. The proposed steps for PhCH_2OH dehydrogenation on $\text{Pt}/\text{MnO}_2\text{-}r$ model.

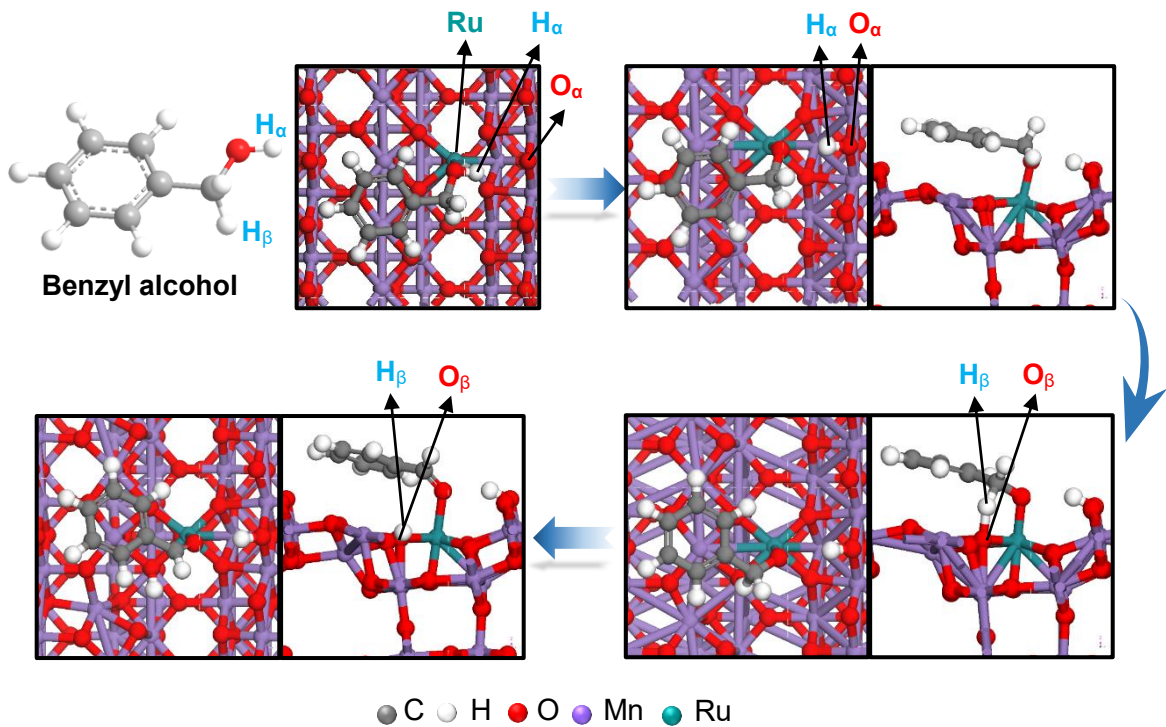


Figure S25. The proposed steps for PhCH_2OH dehydrogenation on $\text{Ru/MnO}_2\text{-}r$ model.

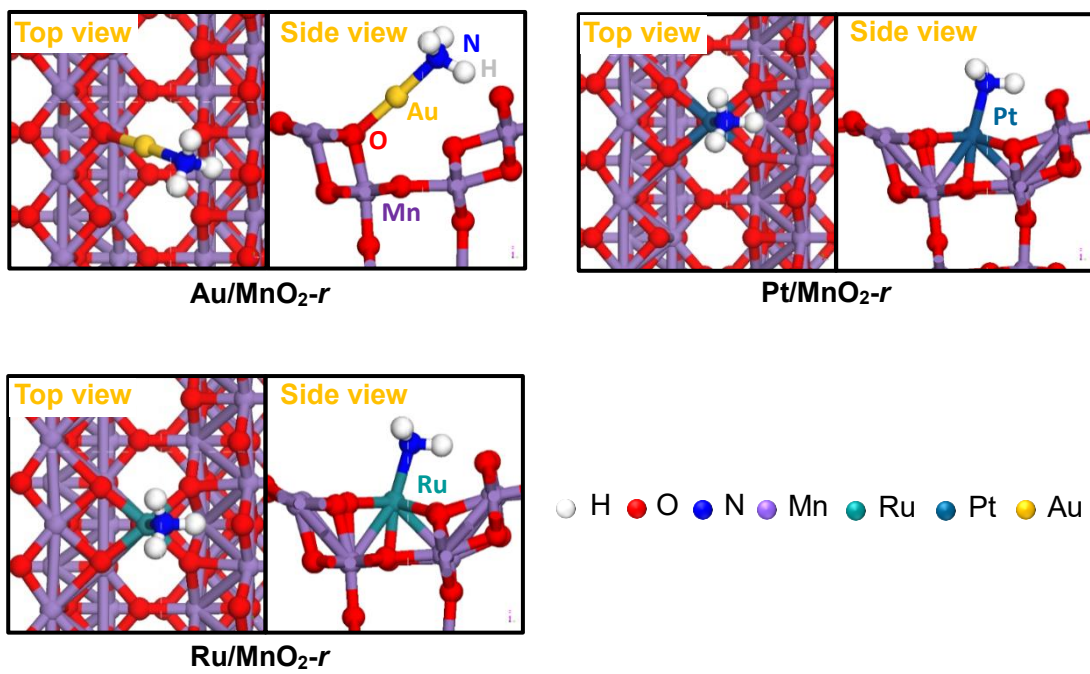


Figure S26. The models of NH₃ adsorbed on the Au-containing, Pt-containing, and analogous Ru/MnO₂-*r* catalysts.

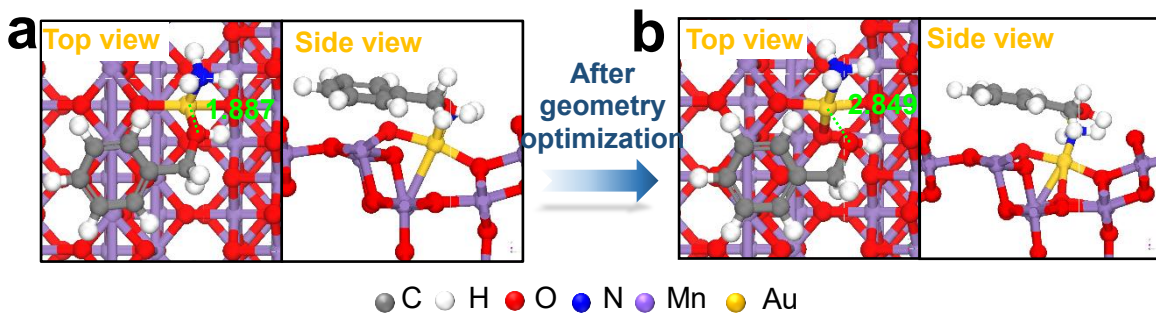


Figure S27. Co-adsorption structures of NH_3 and benzyl alcohol at the Au site over Au/MnO_2-r before (a) and after (b) geometry optimization.

Note: It is possible that the ammonia molecule adsorbs on the Au sites with benzyl alcohol pre-adsorbed (Figure S27a); however, the resulting co-adsorption system is unstable in this case, and the benzyl alcohol molecule tends to desorb from the Au site after optimization (Figure S27b). These results suggest that the benzyl alcohol molecules are difficult to adsorb on the Au catalyst surface when ammonia co-exist there, which is the main reason for the poor catalytic performance in oxidative cyanation. Therefore, the calculation of the C–H cleavage barrier for the $\text{Au} + \text{NH}_3$ case was not considered in Figure 6b.

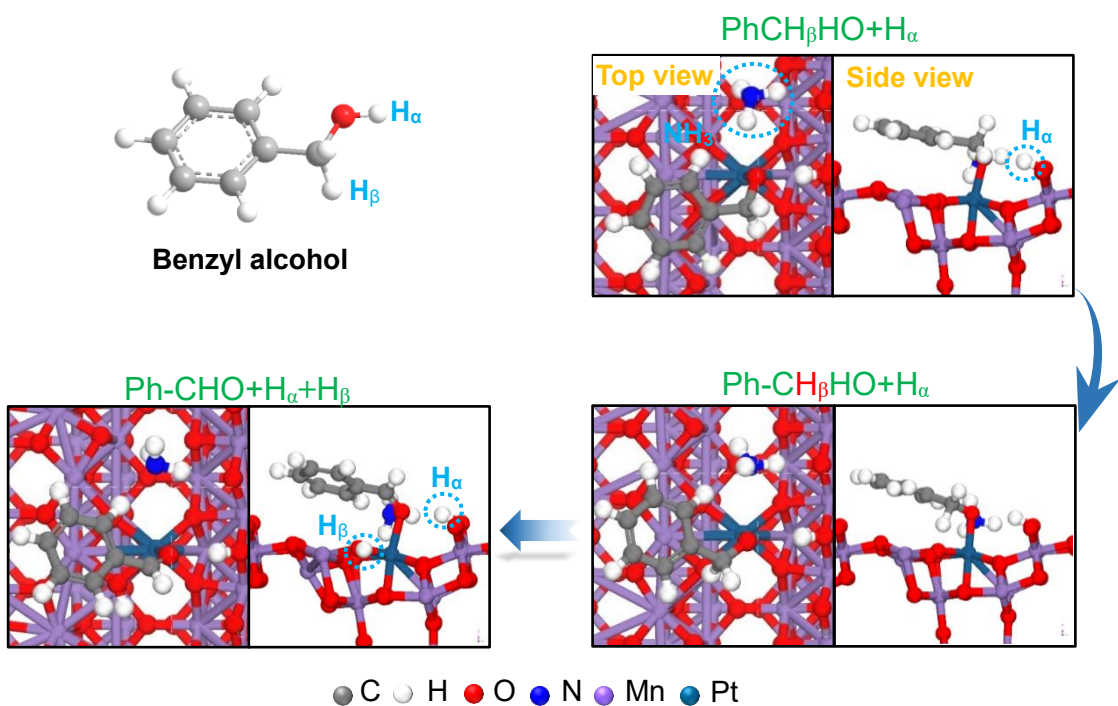


Figure S28. The proposed PhCH_2OH dehydrogenation steps on Pt/MnO_2-r catalyst with the existence of co-adsorbed ammonia molecule ($\text{Pt} + \text{NH}_3/\text{MnO}_2-r$).

Note: When a benzyl alcohol molecule is pre-adsorbed on the Pt site, the NH_3 molecule occupies on the neighboring oxygen species of the Pt atom, which might result in the hindrance of the benzyl alcohol activation because the unavailability of the active oxygen species for C–H bond cleavage, as confirmed by the increased energy barrier for the C–H bond cleavage (Figure 6b).

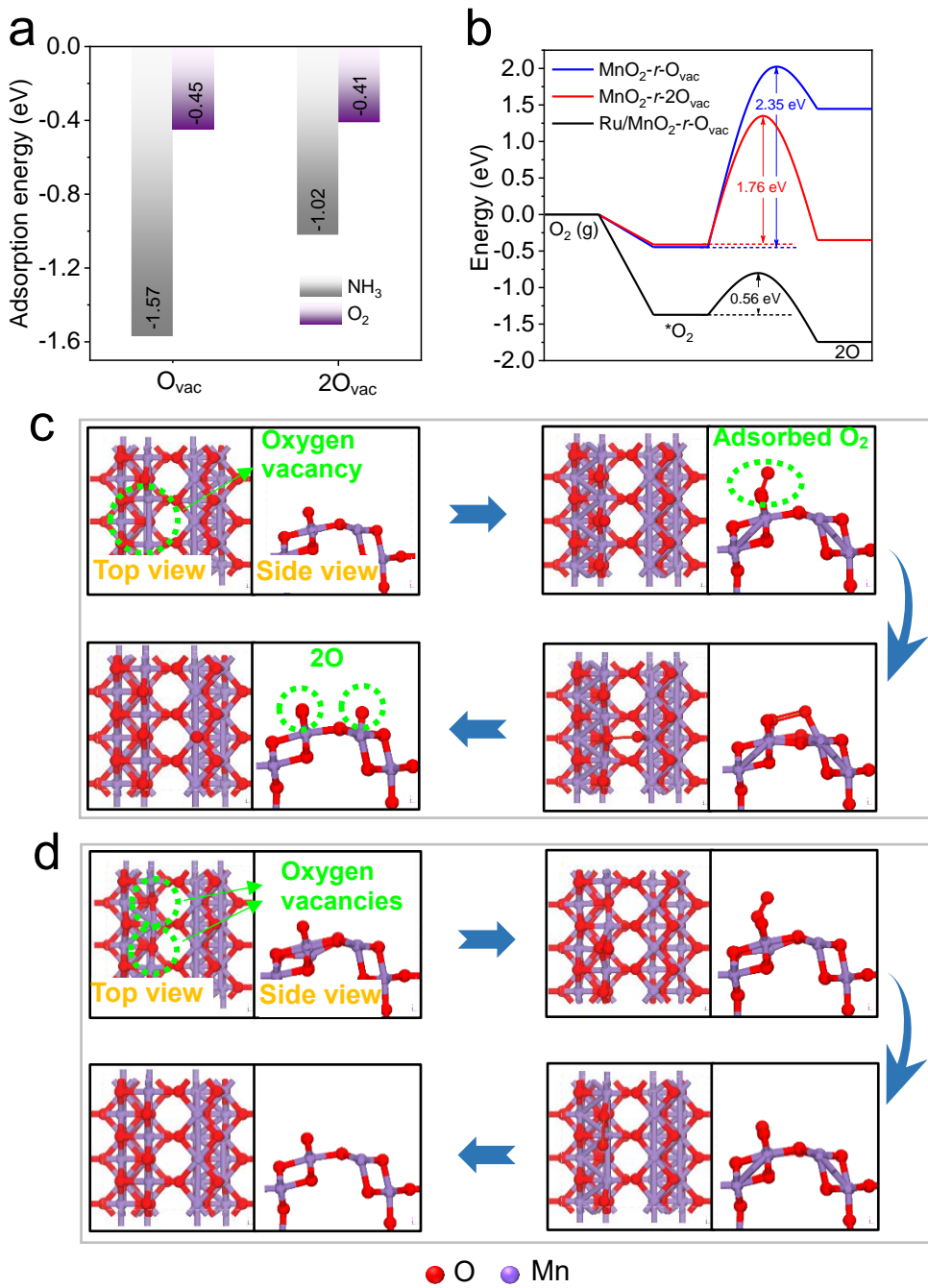


Figure S29. (a) Adsorption energies of NH_3 and O_2 on MnO_2-r with one oxygen vacancy (O_{vac}) and two oxygen vacancies ($2O_{vac}$) near an Mn site. (b) Energy profiles for O_2 adsorption and dissociation on MnO_2-r-O_{vac} , MnO_2-r-2O_{vac} , and Ru/MnO_2-r-O_{vac} . The proposed O_2 adsorption and dissociation steps on (c) MnO_2-r-O_{vac} and (d) MnO_2-r-2O_{vac} .

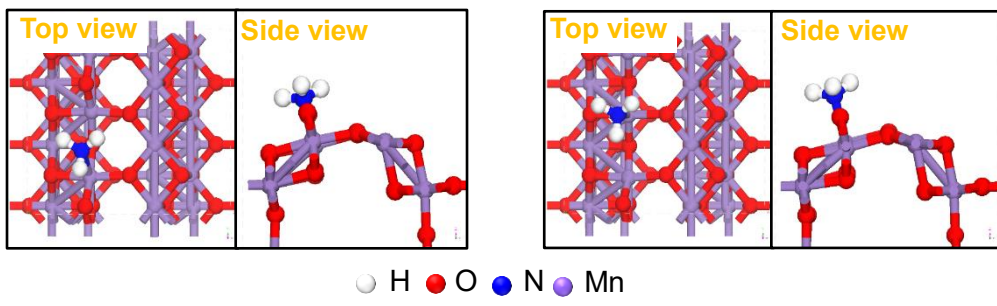


Figure S30. The models of NH_3 adsorbed on the $\text{MnO}_2\text{-}r\text{-O}_{\text{vac}}$ and $\text{MnO}_2\text{-}r\text{-}2\text{O}_{\text{vac}}$.

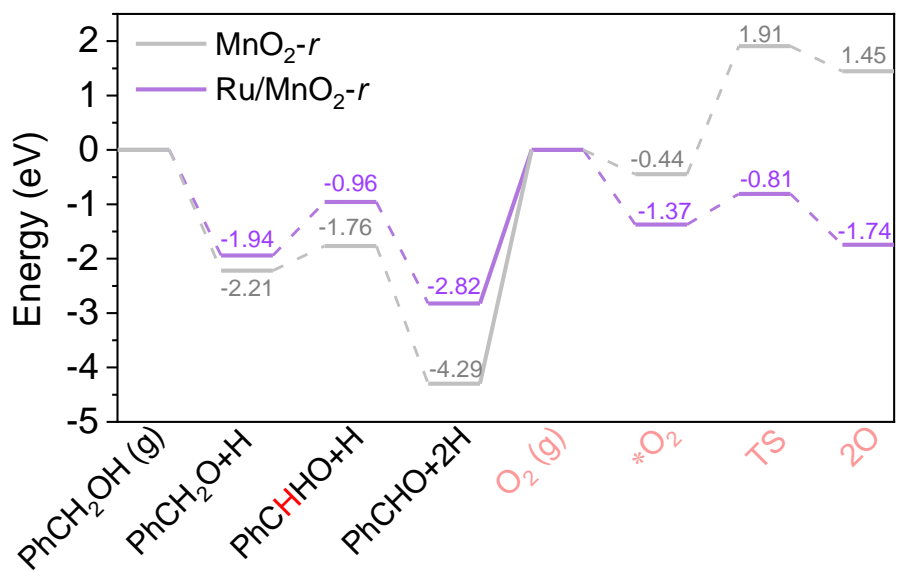


Figure S31. The reaction profile of benzyl alcohol dehydrogenation and molecular oxygen dissociation on MnO_2-r and Ru/MnO_2-r .

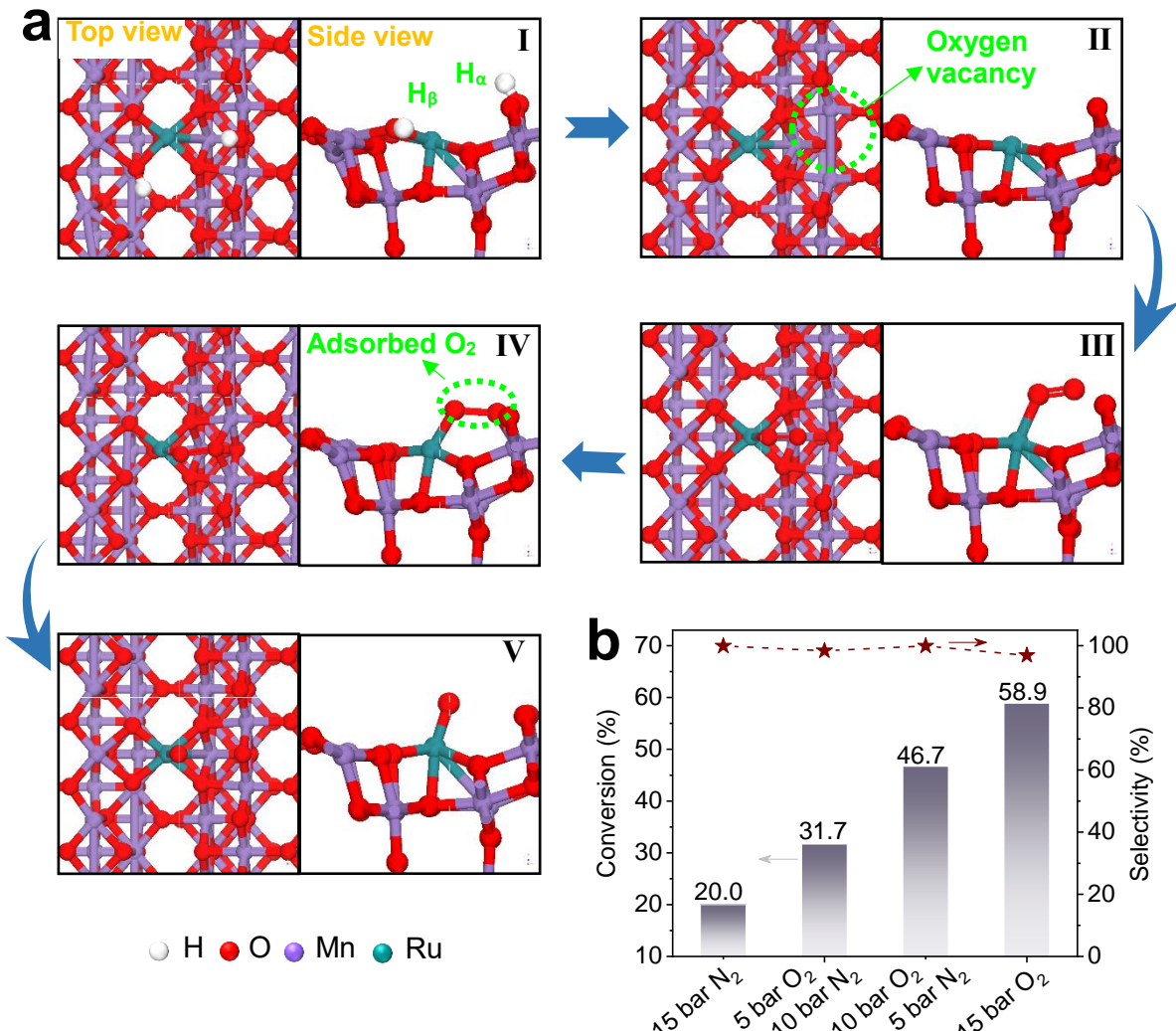


Figure S32. (a) The proposed oxygen vacancy formation and replenishment process on Ru/MnO₂-r catalyst and (b) oxidative cyanation of *n*-heptanol catalyzed by 0.1Ru/MnO₂-r under various atmospheres. Reaction conditions: 0.2 mmol of substrate, 4 mL of *t*-amyl alcohol solvent, 100 μ L of aqueous NH₃ (28–30 wt%), 100 mg of catalyst, 100 °C, 2 h. Selectivity: selectivity to heptanonitrile.

Note: The process of PhCH₂OH to PhCHO proceeds through O-H cleavage first and then C-H dissociation^{20–23}. After the desorption of the final nitrile product from the surface of Ru-MnO₂, two hydrogen atoms (H_α, H_β) will adsorb on the catalyst surface (Figure S32a, step I). We found that the reaction free energy of the removal of these hydrogen atoms with surface oxygen to form H₂O and an oxygen vacancy is -0.20 eV

at the reaction temperature (373 K), indicating that the produced hydrogen (H_α , H_β) can be further removed to form a surface oxygen vacancy on Ru-MnO₂ (step II). Subsequently, O₂ can adsorb on the Ru site due to the enhanced adsorption ability (Figure 6a), and dissociate to O atoms with a barrier 0.56 eV to replenish the oxygen vacancy (step III to V, Figure S31). Furthermore, it is observed that the conversion of *n*-heptanol increased with increasing initial O₂ partial pressure (Figure S32b, Table S10), which should be due to the enhanced oxygen vacancy replenishment.²¹

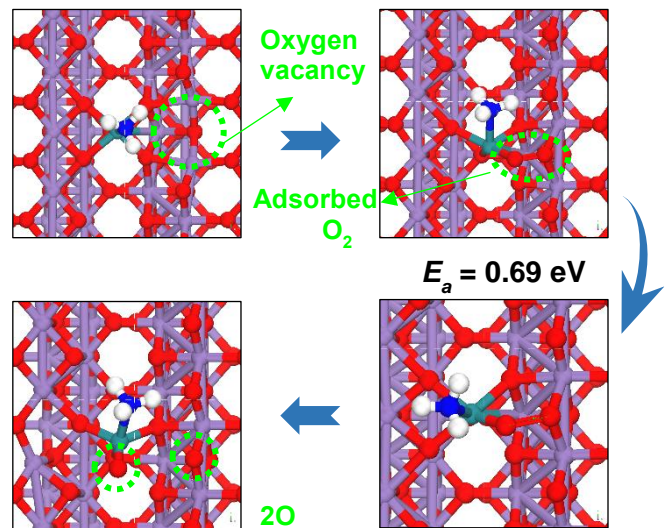


Figure S33. Models showing the oxygen activation on the Ru/MnO₂-r with the presence of ammonia.

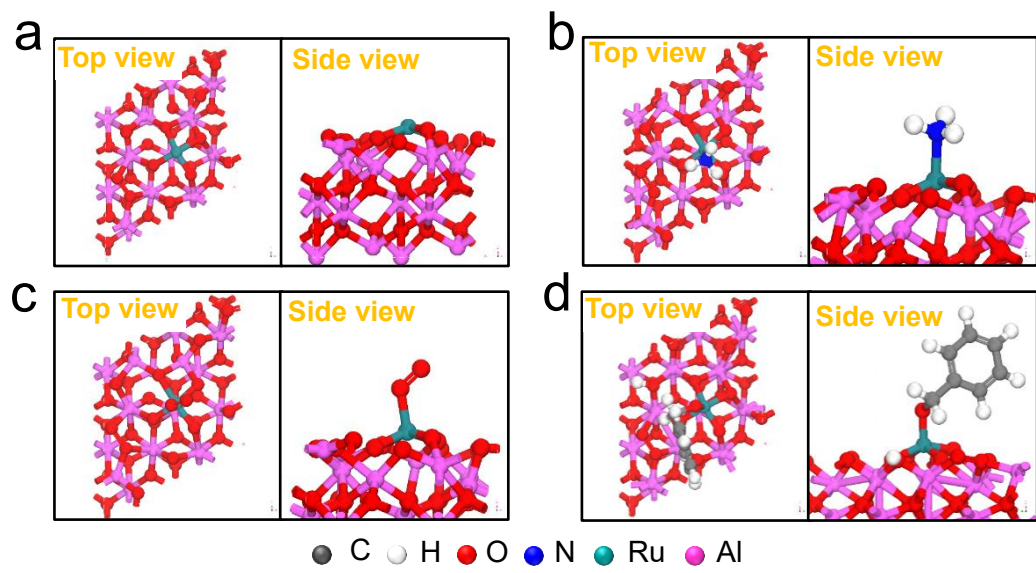


Figure S34. (a) The optimized structure of single-site Ru anchored on Al_2O_3 . The models of (b) NH_3 , (c) O_2 , and (d) benzyl alcohol adsorbed single-site Ru/ Al_2O_3 .

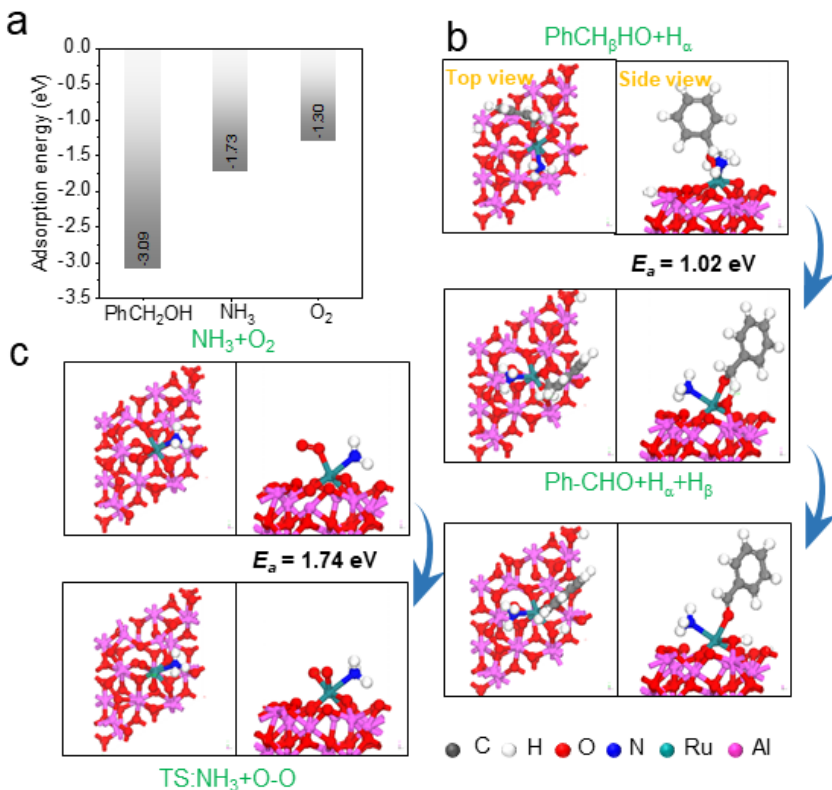
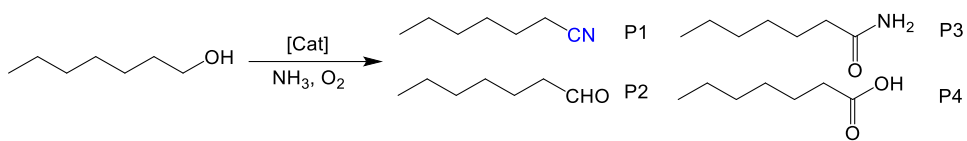


Figure S35. (a) Adsorption energies of PhCH₂OH, NH₃, and O₂ on Ru/Al₂O₃. (b) The proposed PhCH₂OH dehydrogenation steps on Ru/Al₂O₃ catalyst with pre-adsorbed NH₃. (c) The dissociation of molecular oxygen on Ru/Al₂O₃ catalyst with pre-adsorbed NH₃.

Note: Over Ru/Al₂O₃, the activation barrier for the further cleavage of the C-H bond and dissociation of molecular oxygen is 1.02 eV and 1.74 eV, respectively, in the presence of ammonia. One can find that over Ru/Al₂O₃, the dissociation of oxygen is much more difficult than that over Ru/MnO₂-*r* with an activation energy as low as 0.69 eV (Figure S33). These results are in agreement with the experimentally low activity of Ru/Al₂O₃ catalyst in the oxidative cyanation.

Table S1. Catalytic data characterizing oxidative cyanation of *n*-heptanol.[†]

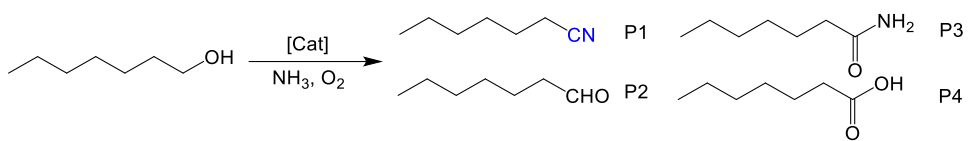
Catalyst	Conv. (%)	Sel. (%)				Balance (%) [§]
		P1	P2	P3	P4	
1	Blank	<0.1	n.d.	n.d.	n.d.	>99.5
2	MnO ₂ - <i>r</i>	40.7	94.3	<0.1	<0.1	n.d. 94.3
3	0.3Au/MnO ₂ - <i>r</i>	32.4	>99.5	<0.1	<0.1	n.d. >99.5
4	0.3Pt/MnO ₂ - <i>r</i>	35.8	90.5	<0.1	<0.1	n.d. 90.5
5	0.3Pd/MnO ₂ - <i>r</i>	35.9	93.0	<0.1	<0.1	n.d. 93.0
6	0.3Rh/MnO ₂ - <i>r</i>	35.1	88.3	<0.1	<0.1	n.d. 88.3
7	0.3Ag/MnO ₂ - <i>r</i>	39.9	93.0	<0.1	<0.1	n.d. 93.0
8	0.3Fe/MnO ₂ - <i>r</i>	33.5	91.6	<0.1	<0.1	n.d. 91.6
9	0.3Ru/MnO ₂ - <i>r</i>	66.9	>99.5	<0.1	<0.1	n.d. >99.5
10	0.01Ru/MnO ₂ - <i>r</i>	38.3	>99.5	<0.1	<0.1	n.d. >99.5
11	0.1Ru/MnO ₂ - <i>r</i>	58.3	>99.5	<0.1	<0.1	n.d. >99.5
12	3.0Ru/MnO ₂ - <i>r</i>	88.5	75.6	<0.1	<0.1	n.d. 75.6
13 [‡]	0.1Ru/MnO ₂ - <i>r</i>	82.4	98.3	<0.1	<0.1	n.d. 98.3
14 [‡]	0.1Ru/MnO ₂ - <i>r</i>	89.1	85.5	<0.1	<0.1	n.d. 85.5

[†]Reaction conditions: 0.2 mmol of substrate, 4 mL of *t*-amyl alcohol solvent, 100 µL of aqueous NH₃ (28-30 wt%), 100 mg of catalyst, 2.0 MPa of oxygen, 100 °C, 2 h. Conv., conversion; Sel., selectivity. n.d.: not detected.

[§]Carbon balance before and after the reaction. The lost carbon is CO₂ from over oxidation.

[‡]5 h.

[‡]6 h.

Table S2. Catalytic data characterizing oxidative cyanation of *n*-heptanol[†].

Catalyst	Conv. (%)	Sel. (%)				Balance (%) [§]
		P1	P2	P3	P4	
1 0.1Ru/CeO ₂	<0.1	n.d.	<0.1	<0.1	n.d.	>99.5
2 0.1Ru/MnO	<0.1	n.d.	<0.1	<0.1	n.d.	>99.5
3 0.1Ru/A-MnO ₂	<0.1	n.d.	<0.1	<0.1	n.d.	>99.5
4 0.1Ru/Co ₃ O ₄	<0.1	<0.1	<0.1	<0.1	n.d.	>99.5
5 0.1Ru/Mn ₃ O ₄	<0.1	n.d.	<0.1	<0.1	n.d.	>99.5
6 0.1Ru/Mn ₂ O ₃	<0.1	<0.1	<0.1	<0.1	n.d.	>99.5
7 0.1Ru/MnO ₂ - <i>r</i>	58.3	>99.5	<0.1	<0.1	n.d.	>99.5

[†]Reaction conditions: 0.2 mmol of substrate, 4 mL of t-amyl alcohol solvent, 100 µL of aqueous NH₃ (28-30 wt%), 100 mg of catalyst, 2.0 MPa of oxygen, 100 °C, 2 h. Conv., conversion; Sel., selectivity. n.d.: not detected.

[§]Carbon balance before and after the reaction.

Table S3. Surface areas of catalyst samples.

Entry	Sample	S _{BET} (m ² /g)
1	MnO ₂ - <i>r</i>	250.5
2	CeO ₂	14.0
3	Co ₃ O ₄	15.0
4	A-MnO ₂	1.6
5	Al ₂ O ₃	72.9
6	SiO ₂	15.5
7	activated carbon	178.6

S_{BET}: BET specific surface area.

Table S4. Comparison of 0.1Ru/MnO₂-*r* with the reported Cu, Fe, and Co-containing catalysts in the nitrile synthesis.

Entry	Product	Catalyst	Temp. (°C)	Time (h)	Yield (%)
1		0.1Ru/MnO ₂ - <i>r</i>	100.0	5.0	>99.0
		Fe-phenanthroline/C	130.0	18.0	98.0
		Co-phenanthroline/C	130.0	18.0	98.0
2		0.1Ru/MnO ₂ - <i>r</i>	100.0	4.0	>99.0
		Fe-phenanthroline/C	130.0	20.0	93.0
		Co-phenanthroline/C	130.0	20.0	95.0
3		0.1Ru/MnO ₂ - <i>r</i>	100.0	3.0	>99.0
		Fe-phenanthroline/C	130.0	20.0	97.0
		Co-phenanthroline/C	130.0	20.0	96.0
4		0.1Ru/MnO ₂ - <i>r</i>	100.0	4.0	>99.0
		Fe-phenanthroline/C	130.0	20.0	98.0
		Co-phenanthroline/C	130.0	20.0	99.0
5		0.1Ru/MnO ₂ - <i>r</i>	100.0	5.0	>99.0
		Fe-phenanthroline/C	130.0	24.0	85.0
		Co-phenanthroline/C	130.0	24.0	86.0
6		0.1Ru/MnO ₂ - <i>r</i>	100.0	5.0	>99.0
		Fe-phenanthroline/C	130.0	20.0	93.0
		Co-phenanthroline/C	130.0	20.0	92.0
		5 mol% of CuI, bpy, TEMPO	50.0	24	98.0
		0.1Ru/MnO ₂ - <i>r</i>	100.0	24.0	>99.0
7		Fe-phenanthroline/C	140.0	26.0-30.0	62.0
		Co-phenanthroline/C	140.0	26.0-30.0	80.0
		5 mol% of CuI, bpy, TEMPO	50.0	24	86.0
		0.1Ru/MnO ₂ - <i>r</i>	100.0	8.0	95.3
9 [†]		Co-phenanthroline/C	130.0	20.0-30.0	93.0
		0.1Ru/MnO ₂ - <i>r</i>	100.0	16.0	96.2
10 [†]		Co-phenanthroline/C	130.0	20.0-30.0	95.0

11 [†]		0.1Ru/MnO ₂ - <i>r</i>	100.0	6.0	93.6
		Co-phenanthroline/C	130.0	20.0-30.0	94.0

Reaction conditions for 0.1Ru/MnO₂-*r*: 0.4 mmol of substrate, 4 mL of *t*-amyl alcohol, 100 µL of aqueous NH₃ (28-30 wt%), 5.0 bar of oxygen, 10 mg of catalyst (0.025 mol% Ru), 100 °C.

[†]Gram scale synthesis of nitriles, 1g of substrate, 60 mL of *t*-amyl alcohol, 100 µL of aqueous NH₃ (28-30 wt%) for each 0.4 mmol substrate, 0.1Ru/MnO₂-*r* (0.025 mol% Ru), 5.0 bar of oxygen, 100 °C.

Reaction conditions for Cu catalyst²³: 1.0 mmol of alcohol, 2 mL of solvent, oxygen balloon, 24 h, 5mol% CuI.

Reaction conditions for Fe-/Co-carbide catalysts²⁴: 0.5 mmol of substrate, 4 mL of *t*-amyl alcohol, weight of catalyst corresponds to 4.0-4.5 mol% metal (metal:phenanthroline = 1:2, in case of Fe = 1:3), 100 µL of aqueous NH₃ (28-30 wt%), 5.0 bar of oxygen, 130 °C.

Note: The data of the previously reported catalysts are from references 23 and 24. Although the homogenous CuI catalyst could work at low temperature, but the bpy and TEMPO additives are needed. In addition, this soluble catalyst has difficulty in separation and regeneration after the reaction²³.

Table S5. Comparison of 0.1Ru/MnO₂-*r* with reported Ru(OH)_x/Al₂O₃ catalyst in the synthesis of various nitriles.

Entry	Product	Catalyst	P _{O₂} (bar)	Temp. (°C)	Time (h)	Yield (%)
1		0.1Ru/MnO ₂ - <i>r</i>	5.0	100.0	5.0	>99.0
		Ru(OH) _x /Al ₂ O ₃	6.0	120.0	5.0	72.0
2		0.1Ru/MnO ₂ - <i>r</i>	5.0	100.0	7.0	>99.0
		Ru(OH) _x /Al ₂ O ₃	6.0	120.0	5.0	80.0
3		0.1Ru/MnO ₂ - <i>r</i>	5.0	100.0	8.0	>99.0
		Ru(OH) _x /Al ₂ O ₃	6.0	120.0	5.0	83.0
4		0.1Ru/MnO ₂ - <i>r</i>	5.0	100.0	5.0	>99.0
		Ru(OH) _x /Al ₂ O ₃	6.0	120.0	5.0	92.0
5		0.1Ru/MnO ₂ - <i>r</i>	5.0	100.0	4.0	>99.0
		Ru(OH) _x /Al ₂ O ₃	6.0	120.0	3.0	96.0
6		0.1Ru/MnO ₂ - <i>r</i>	5.0	100.0	5.0	>99.0
		Ru(OH) _x /Al ₂ O ₃	6.0	120.0	5.0	82.0
7		0.1Ru/MnO ₂ - <i>r</i>	5.0	100.0	5.0	>99.0
		Ru(OH) _x /Al ₂ O ₃	6.0	120.0	7.0	80.0
8		0.1Ru/MnO ₂ - <i>r</i>	5.0	100.0	4.0	>99.0
		Ru(OH) _x /Al ₂ O ₃	6.0	120.0	6.0	81.0

Reaction conditions for 0.1Ru/MnO₂-*r*: 0.4 mmol of substrate, 4 mL of *t*-amyl alcohol, 100 μL of aqueous NH₃ (28–30 wt%), 10 mg of 0.1Ru/MnO₂-*r* (0.025 mol% Ru), 5.0 bar of oxygen, 100 °C.

Reaction conditions for Ru(OH)_x/Al₂O₃²⁵: 0.5 mmol of substrate, 2 mL of 0.45 M THF solution of ammonia, Ru(OH)_x/Al₂O₃ (10 mol% Ru), 6.0 bar of oxygen, 120 °C. The data are from reference 25.

Table S6. Average reaction rate (r_0) in the conversion of benzyl alcohol catalysed by MnO₂-*r*, Ru/MnO₂-*r*, and Ru/Al₂O₃.

Entry	Catalyst	Average reaction rate (mmol g _{cat} ⁻¹ h ⁻¹)	
		NH ₃ on	NH ₃ off
1	MnO ₂ - <i>r</i>	11.5	18.6
2	Ru/MnO ₂ - <i>r</i>	25.0	24.7
3	Ru/Al ₂ O ₃	<0.1	<0.1

Reaction conditions: 0.4 mmol of substrate, 4 mL of *t*-amyl alcohol solvent, 100 µL of aqueous NH₃ (28-30 wt%), 1.5 MPa of oxygen, 75 °C.

Table S7. Average reaction rates in the conversion of benzyl alcohol on MnO₂-*r*, Ru/MnO₂-*r*, and Ru/Al₂O₃.

Entry	Catalyst	Average reaction rate normalized per mole of Ru (mol mol _{Ru} ⁻¹ h ⁻¹)		Average reaction rate normalized to surface area (mmol m ² _{cat} ⁻¹ h ⁻¹)	
		NH ₃ on	NH ₃ off	NH ₃ on	NH ₃ off
1	MnO ₂ - <i>r</i>	-	-	0.05	0.07
2	Ru/MnO ₂ - <i>r</i>	2526.8	2496.5	0.10	0.10
3	Ru/Al ₂ O ₃	<0.1	<0.1	<0.1	<0.1

Reaction conditions: 0.4 mmol of substrate, 4 mL of *t*-amyl alcohol solvent, 100 µL of aqueous NH₃ (28-30 wt%), 1.5 MPa of oxygen, 75 °C.

Table S8. Energy barriers for PhCH₂OH dehydrogenation on various catalysts.

Dehydrogenation Steps	Au/MnO ₂ - <i>r</i>		Pt/MnO ₂ - <i>r</i>		Ru/MnO ₂ - <i>r</i>	
	<i>Ea</i>	ΔE	<i>Ea</i>	ΔE	<i>Ea</i>	ΔE
PhCH _β HOH _α → PhCH _β HO+H _α	/	-2.32	/	-3.62	/	-3.63
PhCH _β HO+H _α → PhCHO+H _α H _β	0.46	-1.85	0.91	-1.14	0.93	-1.06

Table S9. Energy barriers for PhCH₂OH dehydrogenation on various catalysts.

Dehydrogenation Steps	Pt+NH ₃ /MnO ₂ - <i>r</i>	Ru+NH ₃ /MnO ₂ - <i>r</i>		
	Ea	ΔE	Ea	ΔE
PhCH _β HOH _α → PhCH _β HO+H _α	/	-1.22	/	-1.94
PhCH _β HO+H _α → PhCHO+H _α H _β	1.25	-1.08	0.98	-0.88

Table S10. Catalytic data characterizing oxidative cyanation of *n*-heptanol under various atmospheres.[†]

Catalyst	Atmosphere	Conv. (%)	Sel. (%)				Balance (%) [§]
			P1	P2	P3	P4	
1	0.1Ru/MnO ₂ - <i>r</i>	58.9	97.0	<0.1	<0.1	n.d.	97.0
2	O ₂ (1.0 MPa)	46.7	>99.5	<0.1	<0.1	n.d.	>99.5
	N ₂ (0.5 MPa)						
3	O ₂ (0.5 MPa)	31.7	98.4	<0.1	<0.1	n.d.	98.4
	N ₂ (1.0 MPa)						
4	N ₂ (1.5 MPa)	20.0	>99.5	<0.1	<0.1	n.d.	>99.5

[†]Reaction conditions: 0.2 mmol of substrate, 4 mL of *t*-amyl alcohol solvent, 100 μL of aqueous NH₃ (28–30 wt%), 100 mg of catalyst, 100 °C, 2 h. Sel., selectivity. n.d.: not detected.

[§]Carbon balance before and after the reaction.

References

- (1) Liu, Y.; Zhang, M.; Zhang, J.; Qian, Y. A Simple Method of Fabricating Large-Area α -MnO₂ Nanowires and Nanorods. *J. Solid State Chem.* **2006**, *179*, 1757-1761.
- (2) Luo, J.; Zhu, H. T.; Fan, H. M.; Liang, J. K.; Shi, H. L.; Rao, G. H.; Li, J. B.; Du, Z. M.; Shen, Z. X. Synthesis of Single-Crystal Tetragonal α -MnO₂ Nanotubes. *J. Phys. Chem. C* **2008**, *112*, 12594-12598.
- (3) Zhou, J.; Qin, L.; Xiao, W.; Zeng, C.; Li, N.; Lv, T.; Zhu, H. Oriented Growth of Layered-MnO₂ Nanosheets over α -MnO₂ Nanotubes for Enhanced Room-Temperature HCHO Oxidation. *Appl. Catal. B* **2017**, *207*, 233-243.
- (4) Rong, S.; Zhang, P.; Liu, F.; Yang, Y. Engineering Crystal Facet of α -MnO₂ Nanowire for Highly Efficient Catalytic Oxidation of Carcinogenic Airborne Formaldehyde. *ACS Catal.* **2018**, *8*, 3435-3446.
- (5) Fu, Q.; Saltsburg, H.; Flytzani-Stephanopoulos, M. Active Nonmetallic Au and Pt Species on Ceria-Based Water-Gas Shift Catalysts. *Science* **2003**, *301*, 935-938.
- (6) Herzing, A. A.; Kiely, C. J.; Carley, A. F.; Landon, P.; Hutchings, G. J. Identification of Active Gold Nanoclusters on Iron Oxide Supports for CO Oxidation *Science* **2008**, *321*, 1331-1335.
- (7) Zhai, Y.; Pierre, D.; Si, R.; Deng, W.; Ferrin, P.; Nilekar, A. U.; Peng, G.; Herron, J. A.; Bell, D. C. Saltsburg, H.; Mavrikakis, M.; Flytzani-Stephanopoulos, M. Alkali-Stabilized Pt-OH_x Species Catalyze Low-Temperature Water-Gas Shift Reactions. *Science* **2010**, *329*, 1633-1636.
- (8) Chen, G.; Zhao, Y.; Fu, G.; Duchesne, P. N.; Gu, L.; Zheng, Y.; Weng, X.; Chen, M.; Zhang, P.; Pao, C.-W.; Lee, J.-F.; Zheng, N., Interfacial Effects in Iron-Nickel Hydroxide–Platinum Nanoparticles Enhance Catalytic Oxidation. *Science* **2014**, *344*, 495-499.
- (9) Dvořák, F.; Camellone, M. F.; Tovt, A.; Tran, N.-D.; Negreiros, F. R.; Vorokhta, M.; Skála, T.; Matolínová, I.; Mysliveček, J.; Matolín, V.; Fabris, S. Creating Single-Atom Pt-Ceria Catalysts by Surface Step Decoration. *Nat. Commun.* **2016**, *7*, 10801.
- (10) Guo, L.-W.; Du, P.-P.; Fu, X.-P.; Ma, C.; Zeng, J.; Si, R.; Huang, Y.-Y.; Jia, C.-J.; Zhang, Y.-W.; Yan, C.-H. Contributions of Distinct Gold Species to Catalytic Reactivity for Carbon Monoxide Oxidation. *Nat. Commun.* **2016**, *7*, 13481.

- (11) Wan, J.; Chen, W.; Jia, C.; Zheng, L.; Dong, J.; Zheng, X.; Wang, Y.; Yan, W.; Chen, C.; Peng, Q.; Wang, D.; Li, Y. Defect Effects on TiO₂ Nanosheets: Stabilizing Single Atomic Site Au and Promoting Catalytic Properties. *Adv. Mater.* **2018**, *30*, 1705369.
- (12) Wei, X.; Shao, B.; Zhou, Y.; Li, Y.; Jin, C.; Liu, J.; Shen, W. Geometrical Structure of the Gold–Iron(III) Oxide Interfacial Perimeter for CO Oxidation. *Angew. Chem. Int. Ed.* **2018**, *57*, 11289-11293.
- (13) Fu, X.-P.; Guo, L.-W.; Wang, W.-W.; Ma, C.; Jia, C.-J.; Wu, K.; Si, R.; Sun, L.-D.; Yan, C.-H. Direct Identification of Active Surface Species for Water-Gas Shift Reaction on Gold-Ceria Catalyst. *J. Am. Chem. Soc.* **2019**, *141*, 4613-4623.
- (14) Pereira-Hernández, X. I.; DeLaRiva, A.; Muravev, V.; Kunwar, D.; Xiong, H.; Sudduth, B.; Engelhard, M.; Kovarik, L.; Hensen, E. J. M.; Wang, Y.; Datye, A. K. Tuning Pt-CeO₂ Interactions by High-Temperature Vapor-Phase Synthesis for Improved Reducibility of Lattice Oxygen. *Nat. Commun.* **2019**, *10*, 1358.
- (15) Wang, F.; Ueda, W.; Xu, J. Detection and Measurement of Surface Electron Transfer on Reduced Molybdenum Oxides (MoO_x) and Catalytic Activities of Au/MoO_x. *Angew. Chem. Int. Ed.* **2012**, *51*, 3883-3887.
- (16) Long, J.; Xie, X.; Xu, J.; Gu, Q.; Chen, L.; Wang, X. Nitrogen-Doped Graphene Nanosheets as Metal-Free Catalysts for Aerobic Selective Oxidation of Benzylic Alcohols. *ACS Catal.* **2012**, *2*, 622-631.
- (17) Wang, Y.; Furukawa, S.; Yan, N. Identification of an Active NiCu Catalyst for Nitrile Synthesis from Alcohol. *ACS Catal.* **2019**, *9*, 6681-6691.
- (18) Deng, W.; Wang, Y.; Zhang, S.; Gupta, K. M.; Hülsey, M. J.; Asakura, H.; Liu, L.; Han, Y.; Karp, E. M.; Beckham, G. T.; Dyson, P. J.; Jiang, J.; Tanaka, T.; Wang, Y.; Yan, N. Catalytic Amino Acid Production from Biomass-Derived Intermediates. *Proc. Natl. Acad. Sci. USA* **2018**, *115*, 5093-5098.
- (19) Tompsett, D.; Parker, S.; Islam, M. S. Surface Properties of α-MnO₂: Relevance to Catalytic and Supercapacitor Behaviour. *J. Mater. Chem. A* **2014**, *2*, 15509-15518.
- (20) Zhu, X.; Guo, Q.; Sun, Y.; Chen, S.; Wang, J.-Q.; Wu, M.; Fu, W.; Tang, Y.; Duan, X.; Chen, D.; Wan, Y. Optimising Surface d Charge of AuPd Nanoalloy Catalysts for Enhanced Catalytic Activity. *Nat. Commun.* **2019**, *10*, 1428.
- (21) Li, T.; Liu, F.; Tang, Y.; Li, L.; Miao, S.; Su, Y.; Zhang, J.; Huang, J.; Sun, H.; Haruta, M.; Wang, A.; Qiao, B.; Li, J.; Zhang, T. Maximizing the Number of

- Interfacial Sites in Single-Atom Catalysts for the Highly Selective, Solvent-Free Oxidation of Primary Alcohols. *Angew. Chem. Int. Ed.* **2018**, *57*, 7795-7799.
- (22) Rodriguez, P.; Kwon, Y.; Koper, M. T. M. The Promoting Effect of Adsorbed Carbon Monoxide on the Oxidation of Alcohols on a Gold Catalyst. *Nat. Chem.* **2012**, *4*, 177-182.
- (23) Yin, W.; Wang, C.; Huang, Y. Highly Practical Synthesis of Nitriles and Heterocycles from Alcohols Under Mild Conditions by Aerobic Double Dehydrogenative Catalysis. *Org. Lett.* **2013**, *15*, 1850-1853.
- (24) Jagadeesh R. V.; Junge H.; Beller, M. Green Synthesis of Nitriles Using Non-Noble Metal Oxides-Based Nanocatalysts. *Nat. Commun.* **2014**, *5*, 4123.
- (25) Oishi, T.; Yamaguchi, K.; Mizuno, N. Catalytic Oxidative Synthesis of Nitriles Directly from Primary Alcohols and Ammonia. *Angew. Chem. Int. Ed.* **2009**, *48*, 6286-6288.